Ψ_k Newsletter

AB INITIO (FROM ELECTRONIC STRUCTURE) CALCULATION OF COMPLEX PROCESSES IN MATERIALS

Number 104 April 2011

Editor: Z (Dzidka) Szotek
E-mail: psik-coord@stfc.ac.uk

Sponsored by: UK's CCP9
and Psi-k

Contents

1 Editorial

In this April 2011 issue of the Psi-k Newsletter we would like to turn readers' attention to a very informative scientific highlight article by M. Gradhand (MPI Halle, Germany), D. V. Fedorov (MLU Halle, Germany), F. Pientka (MLU Halle & FU Berlin, Germany), P. Zahn (MLU Halle, Germany), I. Mertig (MLU & MPI, Halle, Germany) and B. L. Gyorffy (Bristol University, UK) on "First-principles calculations of the Berry curvature of Bloch states for charge and spin transport of electrons".

In addition, in this issue we have a report on a recent CP2K Tutorial, as well as, a number of workshop announcements and abstracts of newly submitted or recently published papers. For details, please check the table of content of this issue.

The *Uniform Resource Locator* (URL) for the Psi-k webpage is:

http://www.psi-k.org.uk/

Please note, if you have not noticed yet, that recently this webpage has slightly changed its looks through different headings and distribution of Psi-k related information. As a result, e. g. the Psi-k newsletters and highlights, as well as, the Psi-k Portal appear under "Ψ_k Activities". Of course, the webpage is open to further improvements and we will be happy to receive any suggestions for changes in this respect. Thank you.

Please submit all material for the next newsletters to the email address below.

The email address for contacting us and for submitting contributions to the Psi-k newsletters is

	function
psik-coord@stfc.ac.uk	**messages to the coordinators, editor & newsletter**

Dzidka Szotek, Martin Lüders, Leon Petit and Walter Temmerman
e-mail: psik-coord@stfc.ac.uk

2 Psi-k Activities

”Towards Atomistic Materials Design”

2.1 Reports on the Workshops supported by Psi-k

2.1.1 Report on 2nd CP2K Tutorial: Enabling the Power of Imagination in MD Simulations

ETH Zürich, Hönggerberg

February 7th - 11th, 2011

Sponsored by psi-k and CECAM

Marcella Iannuzzi (University of Zurich, Switzerland), Teodoro Laino (IBM Research - Zurich, Switzerland), Ari Paavo Seitsonen (University of Zurich, Switzerland)

http://www.cecam.org/workshop-529.html

Report

The goal of the CP2K tutorial was to provide researchers and students in the field of molecular simulations a survey of the most relevant computational tools implemented within the CP2K program package (http://cp2k.berlios.de/), and to encourage modular, flexible, and problem oriented thinking while using them. We designed the lectures and practical sessions to let the researchers acquire the knowledge to be able to teach less experienced people in their home institutes. Furthermore, the tutorial provided good networking opportunities: by letting other people working in the molecular simulation field know each other, by meeting distinguished researchers, and by establishing contacts that may lead to research collaborations in the future.

We specifically covered the use of different levels of theory: ab-initio DFT, classical Hamiltonians, semi-empirical NDDO and hybrid QM/MM simulations. Particular attention was paid in presenting these methodologies like they are implemented in CP2K. In a second step, we demonstrated how to apply these levels of theory to several methods - provided by CP2K - for exploring potential and free energy surfaces, to characterise molecular reactions or physical phenomena, in particular: molecular dynamics, band methods, ionic relaxation methods, vibrational analysis, and metadynamics. At the same time we covered the calculation of properties

(NMR, XAS) as well as several other features of the DFT-part of the code, such as hybrid exchange-correlation functionals and DFT dispersion corrections, and more in general the usage of multiple `force_evals` (section specifying the type of theory used to obtain the forces on the ions) which is the core of the flexibility behind the usage of CP2K. Lectures on real-case applications were also proposed, to give a flavour of results that can be obtained by exploiting the features and flexibility of CP2K.

Although brief introductions were provided, both at the different levels of theory and on the explorative tools, the emphasis was placed on their practical usage and the relevant implementation details in CP2K. Therefore, this second tutorial, similarly to the first one, deliberately targeted researchers with experience in fields where the presented techniques are well established, and who already possessed a (strong) background in computational chemistry or physics.

Key lectures

The five days were divided into two parts: morning sessions with lectures and afternoon sessions held on terminals where the participants could practice with prepared exercises, or alternatively with their own research projects.

The lectures of the first days concentrated on general algorithms and methods. In the subsequent days the lectures concentrated more on specific and detailed methodologies. On the last day short presentations delivered by some of the participants gave an overview of scientific topics in which CP2K has either already been applied to or that could potentially be used for.

The first day focused on the characteristics and the parallel efficiency in the density functional theory (DFT-)module QuickStep in CP2K (M. Iannuzzi), and a general lecture on error analysis of molecular dynamics algorithms (J. Hutter).

In the terminal session of the afternoon we first introduced the input structure of CP2K. Subsequently we provided 30 molecular structures that could be used by the participants to practice energy and force calculations, and geometry optimisations. Due to the limited computational power available, we encouraged the participants to use semi-empirical Hamiltonians, classical force fields (provided for some of the molecular structures), and in few cases DFT. The high flexibility of the code allows a deep understanding of its methodologies even without the need of using a DFT Hamiltonian.

The lectures of the second day focused on the semi-empirical methods implemented in CP2K (T. Laino), the X-ray absorption and nuclear magnetic resonance spectroscopy spectroscopies (M. Iannuzzi), and the van der Waals/dispersion force schemes (A.P. Seitsonen) currently implemented in CP2K/QuickStep. The afternoon session continued with general examples aimed at familiarising with different methodological modules: `GEO_OPT` (the geometry optimisation module), MD (the molecular dynamics module). All the examples were executed, similarly to the first day, employing several kinds of Hamiltonians.

This way, during the first two days we built the infrastructure in order to focus in the subsequent days on more elaborate topics, namely either different Hamiltonians or various MD methodologies.

The main topics of the lectures on the third day were ensembles and thermostats in the molecular dynamics simulations (G. Bussi), Monte Carlo simulation of liquid/vapour interfaces (W. Kuo because Matthew McGrath was not able to come), classical Force Fields (W. Kuo), and QM/MM methods (T. Laino). The afternoon sessions were organised in a different way compared to the first two days: Instead of working on simple molecular systems, we provided real-case scenarios where the different methodologies presented during the whole week were extensively used. We provided all needed files to set up the problem, input files as well as output files. These examples being real case studies, most of the exercises would have required computational resources beyond the ones available for the tutorial. Nonetheless, we found that these examples, on which participants worked for the rest of the week, were extremely instructive: Participants had the opportunity to see input files prepared by expert users, check the generated output, and have examples on post-processing. Each participant was free to work on the favourite topics, and pose related questions to the experts present. Many of the participants, starting from the given examples, could initialise the CP2K-setup for research problems they want to investigate. At the end of the week, the participants had an overview on how CP2K features can be exploited in a fruitful way.

In the fourth and fifth day we covered potential energy (T. Laino) and free energy (M. Iannuzzi) exploration tools by presenting nudged-elastic band methods and the metadynamics. We further demonstrated state-of-the-art applications of CP2K at surfaces and interfaces: on self-assembly (C. Pignedoli) and adsorption of molecules on metallic surfaces (G. Santarossa), dye-sensitised solar cells (F. Schiffmann) on oxide surfaces, and graphene (A.P. Seitsonen) on a semi-conducting substrate. The short talks by nine participants on their research topics concluded the lecture sessions.

Feedback

All the students gave a very good evaluation of the tutorial, shown either during the hands-on part of the tutorial or during their presentation time. We note that this is a remarkable result, since more than 40 % of the attendees were researchers or lecturers with considerable teaching experience. The idea of giving the participants the opportunity to show their research problems was also extremely useful to us to understand what people find most useful in the code and what they miss. Several presenters had already a clear idea on how to employ the CP2K package once back at home to solve their problems, and a few people showed also interest in implementing features currently missing in CP2K that would become useful in their research activity.

A general remark was made about the computational power available for the tutorial. Although the general part of the hands-on exercises were tuned in order to run on commodity desktops, most of the attendees would have been pleased by a larger computational power. In fact, while the need for computational resources was not an issue for the first two afternoon sessions, it it would have been highly required (although we provided output files) for the last 3 afternoons.

Overall the tutorial can be considered to be very successful. We could attract expert researchers as we received an overwhelming number of applications from all over the world. Individual feedbacks collected by one-to-one questions indicate that the program was of high value, very interesting and useful for the participants. Several students remarked the particular value of the hands-on part.

Our major concern was being forced to reject more than two times the number of accepted participants. The interest in CP2K is clearly growing year by year and we strongly stress the need for such tutorials that do not focus entirely on one specific topic or methodology but rather on the full capability of a simulation package. We believe that a series of tutorials on different computational packages (including CP2K itself) would be extremely useful for the scientific community. Our wish is that both the satisfaction of the participants and the interest shown for the code (more than 85 applications) will be convincing arguments for having the 3rd CP2K tutorial in 2013.

Programme

Day 1 - February 7th

- Welcome
  - 08:30 to 08:45
- Methods for DFT electronic structure calculations
  - 08:45 to 09:35 - Marcella Iannuzzi: GPW and GAPW electronic structure calculations
- High performance computing
  - 09:45 to 10:30 - Urban Borštnik: High performance computing with CP2K
- Advanced DFT methods: hybrid functionals
  - 11:00 to 11:50 - Joost VandeVondele: Hybrid functionals
- Ab initio molecular dynamics: BO vs CP
  - 12:00 to 12:50 - Jürg Hutter: Methods for ab initio molecular dynamics
- Hands-on: starting up, using GPW with different functionals, `GEO_OPT` and AIMD
  - 14:00 to 18:30 - Exercises

Day 2 - February 8th

- Semiempirical Hamiltonian
  - 08:30 to 09:20 - I-Feng William Kuo: Force fields and molecular mechanics
  - 09:30 to 10:30 - Teodoro Laino: NDDO
- Properties
  - 11:00 to 12:00 - Marcella Iannuzzi: Core level Spectroscopy and NMR
  - 12:00 to 12:50 - Ari Paavo Seitsonen: van der Waals corrections in approximative DFT-KS functionals
- Hands-on: FF, DFT properties, vdW, semiempirical methods
  - 14:00 to 18:30 - Exercises

Day 3 - February 9th

- Sampling
  - 08:30 to 09:20 - Giovanni Bussi: MD ensembles and thermostats
  - 09:30 to 10:20 - Matthew McGrath: MC simulations of liquid/vapour interfaces
- QM/MM
  - 11:00 to 12:00 - Teodoro Laino: QM/MM methods
  - 12:00 to 13:00 - I-Feng William Kuo: MM and QM/MM for bio applications
- Hands-on: real systems simulations
  - 14:00 to 18:30 - Exercises
- 20:00 to 23:00 - Conference dinner

Day 4 - February 10th

- Rare events: bands methods
  - 08:30 to 09:30 - Marcella Iannuzzi: Free energy calculations by MD
  - 09:30 to 10:30 - Gianluca Santarossa: Structural rearrangement and catalytic processes
- Applications
  - 11:00 to 12:00 - Marcella Iannuzzi: Metallic interfaces and nanomesh
  - 12:00 to 13:00 - Teodoro Laino: Band methods
- Hands-on: real systems simulations
  - 14:00 to 18:00 - Exercises

Day 5 - February 11th

- Large systems multiscale applications
  - 08:30 to 09:30 - Carlo Antonio Pignedoli: Nanostructures and adsorption on metallic surfaces
  - 09:30 to 10:30 - Florian Schiffmann: Dye sensitised solar cells
- Future challenges
  - 11:00 to 11:30 - Ari Paavo Seitsonen: Graphene and more
  - 11:30 to 11:40 - Alexander Kulesza: Optical properties of metal cluster-biomolecule hybrid systems
  - 11:40 to 11:50 - Giorgio Lanzani: The acquatic chemistry of aluminium: kinetics and dynamics
  - 11:50 to 12:00 - Ling Ge: Solute-solvent and solvent solvent interactions in molecular liquids
  - 12:00 to 12:10 - Volker Haigis: Trace element partitioning between silicate melts

    - 12:10 to 12:20 - An Ghysels: Understanding MOFs framework flexibility by Monte Carlo simulation
    - 12:20 to 12:30 - Jose Gomes: Simulation of the early stages of the synthesis of nanoporous materials
    - 12:30 to 12:40 - John Kattirtzi: Calculating acidity constants of the β-$MnO_2(110)$ surface from density functional theory based molecular dynamics
    - 12:40 to 12:50 - Jennifer Guerard: Using CP2K to estimate reorganisation energies and redox potentials of environmental organic contaminants in aquatic systems
    - 12:50 to 13:00 - Jeffrey McMahon: Finite-temperature and quantum-proton effects in atomic metallic hydrogen
- Hands-on: real systems simulations
    - 14:00 to 18:00 - Exercises

Lectures

Most of the lectures are available at the internet site of the tutorial.

List of participants

- Belgium
    - An Ghysels (Center for Molecular Modeling)
- Colombia
    - Ramiro Cardona (Universidad Nacional de Colombia)
- Finland
    - Giorgio Lanzani (Cewic - Centre of Expertise in the Water Industry Cluster - Thule Institute, University of Oulu)
- France
    - Romain Jonchiere (UPMC)
    - Sébastien Le Roux (Institut de Physique et Chimie des Matriaux de Strasbourg)
- Germany
    - Volker Haigis (Helmholtz-Zentrum Potsdam Deutsches Geoforschungszentrum)
    - Emiliano Ippoliti (German Research School for Simulation Sciences GmbH)
    - Barbara Kirchner (University of Leipzig, Wilhelm-Ostwald Institute of Physical and Theoretical Chemistry)
    - Alexander Kulesza (Freie Universität Berlin, Fachbereich Physik)

  - Maria Eugenia Tucceri (Max Planck Institute for Chemistry)

- Hungary

  - Janos Daru (Chemical Research Center Budapest)

- Ireland

  - Alin Marin Elena (University College Dublin)
  - Mahdi Shirazi (Tyndall National Institute)

- Italy

  - Giovanni Bussi (The International School for Advanced Studies, Trieste)
  - Alessandro Motta (consorzio INSTM)
  - Jacopo Sgrignani (CNR-IOM-DEMOCRITOS)

- The Netherlands

  - Omar Valsson (University of Twente)

- Poland

  - Andrzej Bil (Faculty of Chemistry, University of Wroclaw)

- Portugal

  - Jose Gomes (CICECO, University of Aveiro)

- Spain

  - Jaime Gómez-Díaz (ICIQ, Tarragona)

- Sweden

  - Ida Josefsson (Fysikum, Stockholm University)

- Switzerland

  - Urban Borštnik (Physical Chemistry Institute, University of Zurich)
  - Beat Büsser (ETH Zürich)
  - Julian Garrec (Ecole Polytechnique Federale de Lausanne)
  - Jennifer Guerard (EPFL)
  - Jürg Hutter (University of Zurich)
  - Jaap Kroes (Swiss Federal Institute of Technology Lausanne - EPFL)
  - Hans Peter Lüthi (ETH Zurich)
  - Luis Pegado (PSI - Paul Scherrer Institut)
  - Carlo Antonio Pignedoli (Swiss Federal Laboratories for Materials Testing and Research - EMPA)

  - Gianluca Santarossa (ETH Zurich)
  - Andrea Scaramucci (ETH Zurich)
  - Joost VandeVondele (University of Zurich)

- United Kingdom
  - Ling Ge (Imperial College London)
  - John Kattirtzi (University of Cambridge)
  - Florian Schiffmann (University College London)

- USA
  - I-Feng William Kuo (Lawrence Livermore National Laboratory)
  - Jeffrey McMahon (University of Illinois at Urbana–Champaign)
  - Jim Pfaendtner (University of Washington)

2.2 Psi-k Workshop Announcements

2.2.1 Second Announcement of the Workshop on Self-Interaction Correction: State of the Art and New Directions

September 18, 2011 (evening) to September 21, 2011

Ramada Jarvis Hotel, Chester, UK

Organisers:
Martin Lueders, Leon Petit and Zdzislawa (Dzidka) Szotek (Daresbury Laboratory, UK)

Local administration:
Wendy Cotteril and Shirley Miller (Daresbury Laboratory, UK)

Sponsored by
Psi-k Network and CECAM-Hartree Node (UK)

Motivation

The motivation for this workshop is to review different methodologies and different applications of self-interaction corrected local-density approximation (LDA). The self-interaction error, introduced by local and semi-local approximations to density functional theory (DFT), leads to some dramatic failures of DFT, ranging from wrong predictions in chemical reactions to the failure in describing the insulating state in many transition metal oxides, and qualitatively wrong pictures for lanthanide and actinide compounds. Thirty years ago, Perdew and Zunger (PZ) suggested a remedy for this error, the so-called self-interaction corrected (SIC) local (spin) density (LSD) approximation [Phys. Rev. B23, 5048 (1981)]. During the years that have passed since the publication of this seminal paper, the method has led to a plethora of applications in different fields of physics and chemistry. The original paper also gave rise to a variety of implementations, generalizations, and extensions of the method. It has also become apparent that different branches of SIC have been developed nearly independently of each other, in particular in the field of quantum chemistry and solid state physics, with the experiences/advances gained in one field barely noticed in the other areas. We think that this year's 30th anniversary of the original paper by Perdew and Zunger would be a good opportunity to bring together, for the first time, all the groups that have applied/worked on self-interaction correction, in order to discuss and assess the state of the art of all the different flavours of SIC, share the experiences and identify the most important and burning issues, unsolved problems, and perhaps find a common direction for the future development.

Longer invited talks and ample time for discussion are envisaged to facilitate a successful outcome of the workshop.

Invited Speakers

Hisazumi Akai (Osaka University, Japan)
Björn Baumeier (MPI Mainz, Germany)
Klaus Capelle (Sao Paulo, Brazil)
Aron Cohen (Cambridge, UK)
Olle Eriksson (Uppsala University, Sweden)
Alessio Filippetti (Sardinia, Italy)
Hannes Jonsson (Faculty of Science, VR-II, Univ. of Iceland)
Stephan Kuemmel (University of Bayreuth, Germany)
Nicola Marzari (University of Oxford, UK)
Mark R. Pederson (NRL,USA)
John P. Perdew (Tulane University, USA)
Adrienn Ruzsinszky (Tulane University, USA)
Stefano Sanvito (Trinity College Dublin, Ireland)
Thomas C. Schulthess (ETH Zurich, Switzerland)
Julie B. Staunton (Warwick University, UK)
Eric Suraud (University of Toulouse, France)
Axel Svane (Aarhus University, Denmark)
Takao Tsuneda (Yamanshi University, Japan)

Poster Session

In addition to invited talks a poster session is planned for the first evening of the workshop (September 19) to allow participants to present and discuss their contributed papers.

Webpage

A dedicated web page of this meeting is

`http://www.cse.scitech.ac.uk/cecam_at_daresbury/self-interaction_correction.shtml`

Registration

Please note that the registration to the meeting is now open at the above page.

For more information please contact Shirley Miller at shirley.miller@stfc.ac.uk.

The total number of participants is expected to be between 40 and 50.

All the future information concerning the workshop will be distributed via Psi-k Portal and in the forthcoming Psi-k newsletters.

2.2.2 Psi-k/CECAM/CCP9 Biennial Graduate School in Electronic-Structure Methods

July 10, 2011 - July 16, 2011, Oxford, UK

`http://mml.materials.ox.ac.uk/Support/GraduateSchool2011`

Overview

The Psi-k/CECAM/CCP9 Biennial Graduate School in Electronic-Structure Methods will take place in Oxford from Sunday 10th July until Saturday 16th July 2011. This is a combined theory and hands-on school, with morning sessions dedicated to lectures introducing theory and application of electronic structure methods, and afternoon sessions providing hands-on experience with the relevant codes on a high-performance compute cluster.

The methods covered, demonstration codes and lecturers will be

- Density Functional Theory and Density Functional Perturbation Theory: Quantum Espresso
  - Prof Stefano Baroni (Sissa)
  - Prof Nicola Marzari (Oxford)
  - Dr Davide Ceresoli (Oxford)
  - Dr Nicola Bonini (Oxford)
- Linear scaling: ONETEP
  - Dr Peter Haynes (Imperial College)
  - Dr Arash Mostofi (Imperial College)
  - Dr Chris Skylaris (Southampton)
- Quantum Monte Carlo: CASINO
  - Prof Richard Needs (Cambridge) - tbc
- LMTO:
  - Prof Walter Temmerman (Daresbury Laboratory)

  - Prof Dzidka Szotek (Daresbury Laboratory)
  - Dr Martin Lueders (Daresbury Laboratory)
  - Dr Leon Petit (Daresbury Laboratory)

Further details

There will be a fixed academic participation fee of 100, that includes registration, 6 nights bed-and-breakfast accommodation at The Queen's College (one of the oldest and most atmospheric of the Oxford colleges) and the conference dinner. There will be a poster session to enable participants to present their research. Participants should plan to arrive by the evening of Sunday 10th July and depart on Saturday 16th July.

Registration

Please complete and return the registration form (available on the web page). The application deadline is 3rd May 2011. We will confirm participation shortly after this date, and provide details of how to pay the registration fee.

Organizers

Prof Nicola Marzari (Oxford)
Prof Walter Temmerman (Daresbury Laboratory)
Dr Jonathan Yates (Oxford)
Mrs Katherine Hartwell (Conference Administrator)

3 General Workshop/Conference Announcements

3.1 WIEN2011: The 18th Hands on Workshop on the WIEN2k package

Penn State University, University Park, PA, USA

June 28- July 1, 2011

Prof. J. O. Sofo and the WIEN2k developers team

http://www.mri.psu.edu/conferences/wien/2011/index.asp

The fifth US workshop on the WIEN code (18th in the history of the WIEN code) is a hands-on activity dedicated to teach the use of the WIEN2k Density Functional Theory Package (http://www.wien2k.at). WIEN2k is one of the most popular electronic structure codes using the Full Potential LAPW method.

The workshop is a unique opportunity to learn the use, power and limitations of the package with the tutoring of the authors and developers of the code. The activities will be aimed at graduate students and researchers from industry and academia. The only pre-requisite is to have a basic knowledge of solid state physics and chemistry. It is planned as a four-day activity with lectures on the scientific aspects of the method, applications, hands-on activities on selected examples, and the opportunity to receive a head start on your personal project.

The invited speakers and tutors include:

-Prof. C. Ambrosch-Draxl (Univ. Leoben, Austria)
-Prof. P. Blaha (TU Vienna, Austria)
-Prof. L.D. Marks (Northwestern Univ., USA)
-Dr. X. Rocquefelte (Univ. Nantes, France)
-Prof. K. Schwarz (TU Vienna, Austria)

Chair: Prof. J. O. Sofo (MSC, PennState Univ., USA)

For more information and registration see:

http://www.mri.psu.edu/conferences/wien/2011/index.asp

3.2 Quantum Monte Carlo and the CASINO program VI

Apuan Alps Centre for Physics @ TTI
Vallico Sotto, Tuscany, Italy

Sat 30th July - Sat 6th August 2011

`www.vallico.net/tti/tti.html`

A4 POSTER:
`www.tcm.phy.cam.ac.uk/~mdt26/poster.png`

The sixth international summer school in the series *Quantum Monte Carlo and the CASINO program* will take place during August 2011 at the TTI monastery in the Tuscan Apuan Alps in Italy, organized and hosted by members of Cambridge University physics department's Theory of Condensed Matter Group. The aim of the school is to give students a thorough introduction to quantum Monte Carlo as a method for performing high-quality calculations of the electronic structure of atoms, molecules, and materials. The course is designed for young quantum chemists or theoretical physicists who have no previous experience with this technique, though anyone interested is welcome to take part, including old people.

The monastery is a unique venue where the community spirit and magnificent location have inspired memorable workshops in the past. It is a delightful 16th century building incorporating an ancient church, and is situated in the isolated but spectacular setting of the Tuscan mountain village of Vallico Sotto. The church is fully equipped with relevant presentation and computer technology, and all accommodation is on-site. As with all events at the Institute, formal lectures are restricted to the mornings, and participants are given the freedom and space to think and to contemplate and discuss the issues at hand. In addition to hands-on exercises, a programme of healthy recreational activities will be organized in the afternoons, and it is hoped that by following this strict regime, together with breathing clean mountain air and by preparing and sampling fine Tuscan cuisine, the participant will be able to return home mentally and physically refreshed as well as better informed.

Describing the complex behaviour of materials at the atomic level requires a sophisticated description of the correlated motion of the electrons. Quantum Monte Carlo (QMC) is an increasingly popular and explicitly many-body method with the unusual capability of yielding highly accurate results whilst also exhibiting a very favourable scaling of computational cost with system size. Over the last eighteen years, the Cambridge group have been researching QMC methods and we have created a powerful, general computer program - CASINO - to carry out the calculations. The school will focus both on the basic theory of QMC and on more advanced practical techniques, and will include a thorough introduction to the CASINO program.

A background in density functional theory or similar - though not essential - is normally thought to be useful.

Quantum Monte Carlo and the scaling behaviour of CASINO on the fastest computers in the world were the subject of last month's Psi-k *Scientific Highlight of the Month* review article. See 'Petascale computing opens new vistas for quantum Monte Carlo' by M.J.Gillan, M.D. Towler and D.Alfè, available for download here:

`www.psi-k.org/newsletters/News_103/Highlight_103.pdf`

Instructors will include the main authors of the CASINO program (Dr. Mike Towler, Dr. Neil Drummond and Dr. Pablo López Ríos) and possibly others.

Participants would normally need to book a flight to Pisa airport from where onward transportation will be arranged (though other destinations are possible). Details of previous schools - including photographs - are available under the PUBLIC EVENTS link on the TTI web site.

Those interested should email Mike Towler (mdt26 at cam.ac.uk) for registration and further details.

3.3 Workshops on crystal structure prediction: France (June 2011) and China (August 2011)

We are happy to announce the forthcoming workshops on modern evolutionary algorithms for crystal structure prediction using the USPEX code. For the convenience of the participants, we are organizing two workshops in 2011, one in Europe and one in Asia, at very special locations:

1. 26 June - 1 July 2011, in Poitiers (France): This workshop will be preceded by a hands-on tutorial on DFT for periodic solids (23-25 June 2011, Poitiers).
   Official website: `http://dnnsm2011.conference.univ-poitiers.fr/?lang=en`
2. 2-6 August 2011, in Xi'an (China):
   Official website: `http://han.ess.sunysb.edu/~aoganov/Workshop_China.html`

Registration is now open until 1 June 2011 - see the above websites for details. Registration fees will include only the living costs, and conference materials for the regular participants; costs for the invited speakers will be covered by separately obtained funds. There will be a limited number of fellowships for students.

Both workshops, gathering the leading developers and practitioners of this field, aim at training new users and developers.

Practical sessions, as well as lectures on theoretical background, will focus on the prediction of stable crystal structures (at ambient, as well as high pressure), computational search for materials with desired properties, treatment of multicomponent systems, nanoparticles, and surfaces. There will be ample time for discussions, for starting new research projects, and for short presentations by the participants/students. Both workshops will include an exciting social program.

The two workshops will have somewhat different scientific programs, and it is possible to attend both. The number of places is limited, acceptance is on the 'first come, first served' basis.

Prof. Artem R. Oganov
Department of Geosciences and Department of Physics and Astronomy,
State University of New York, Stony Brook, NY 11794-2100

Phones: (631)-632-1429 (office), x1449 (lab), x8241 (admin. assistant).
Fax (631) 632 8240
E-mail artem.oganov@sunysb.edu
Web-site: `http://mysbfiles.stonybrook.edu/~aoganov`

NEWS: Web-release of the USPEX code: `http://han.ess.sunysb.edu/~USPEX`

NEWS: Special Issue ”Theory of Superhard Materials”:
`http://www.springerlink.com/content/1063-4576/32/3/`

NEWS: Book ”Modern Methods of Crystal Structure Prediction:
`http://eu.wiley.com/WileyCDA/WileyTitle/productCd-3527409394.html`

4 Abstracts

Band convergence and linearization-error correction of all-electron GW calculations: the extreme case of zinc oxide

Christoph Friedrich, Mathias C. Müller, and Stefan Blügel
Peter Grünberg Institut and Institute for Advanced Simulation,
Forschungszentrum Jülich and JARA, 52425 Jülich, Germany

Abstract

Recently, Shih *et al.* [Phys. Rev. Lett. 105, 146401 (2010)] published a theoretical band gap for wurtzite ZnO, calculated with the non-selfconsistent GW approximation, that agreed surprisingly well with experiment while deviating strongly from previous studies. They showed that a very large number of empty bands is necessary to converge the gap. We reexamine the GW calculation with the full-potential linearized augmented-plane-wave method and find that even with 3000 bands the band gap is not completely converged. A hyperbolical fit is used to extrapolate to infinite bands. Furthermore, we eliminate the linearization error for high-lying states with local orbitals. In fact, our calculated band gap is considerably larger than in previous studies, but somewhat smaller than that of Shih *et al.*.

(Phys. Rev. B 83, 081101(R) (2011))
Contact person: c.friedrich@fz-juelich.de

Local exact exchange potentials within the all-electron FLAPW method and a comparison with pseudopotential results

Markus Betzinger[a], Christoph Friedrich[a], Stefan Blügel[a], and Andreas Görling[b]
[a] *Institut für Festkörperforschung and Institute for Advanced Simulation,*
Forschungszentrum Jülich and JARA, D-52425 Jülich, Germany
[b] *Lehrstuhl für Theoretische Chemie, Universität Erlangen-Nürnberg,*
Egerlandstr. 3, D-91058 Erlangen, Germany

Abstract

We present a general numerical approach to construct local Kohn-Sham potentials from orbital-dependent functionals within the all-electron full-potential linearized augmented-plane-wave (FLAPW) method, in which core and valence electrons are treated on an equal footing. As a practical example, we present a treatment of the orbital-dependent exact-exchange (EXX) energy and potential. A formulation in terms of a mixed product basis, which is constructed from products of LAPW basis functions, enables a solution of the optimized-effective-potential (OEP) equation with standard numerical algebraic tools and without shape approximations for the resulting potential. We find that the mixed product and LAPW basis sets must be properly balanced to obtain smooth and converged EXX potentials without spurious oscillations. The construction and convergence of the exchange potential is analyzed in detail for diamond. Our all-electron results for C, Si, SiC, Ge, GaAs semiconductors as well as Ne and Ar noble-gas solids are in very favorable agreement with plane-wave pseudopotential calculations. This confirms the adequacy of the pseudopotential approximation in the context of the EXX-OEP formalism and clarifies a previous contradiction between FLAPW and pseudopotential results.

(Phys. Rev. B 83, 045105 (2011))
Contact person: m.betzinger@fz-juelich.de

The quantum nature of the hydrogen bond

Xin-Zheng Li, Brent Walker, Angelos Michaelides
London Centre for Nanotechnology and Department of Chemistry,
University College London, London WC1E 6BT, U.K.

Abstract

Hydrogen bonds are weak, generally intermolecular bonds, which hold much of soft matter together as well as the condensed phases of water, network liquids, and many ferroelectric crystals. The small mass of hydrogen means that they are inherently quantum mechanical in nature, and effects such as zero point motion and tunneling must be considered, though all too often this is not done. As a prominent example, a clear picture for the impact of quantum nuclear effects on the strength of hydrogen bonds and consequently the structure of hydrogen bonded systems is still absent. Here, we report *ab initio* path-integral molecular dynamics studies on the quantum nature of the hydrogen bond. Through a systematic examination of a wide range of hydrogen bonded systems we show that quantum nuclear effects weaken weak hydrogen bonds but strengthen relatively strong ones. This simple correlation arises from a competition between anharmonic intermolecular bond bending and intramolecular bond stretching. A simple rule of thumb is provided that enables predictions to be made for hydrogen bonded materials in general with merely classical knowledge (such as hydrogen bond strength or hydrogen bond length). Our work rationalizes the influence of quantum nuclear effects, which can result in either weakening or strengthening of the hydrogen bonds, and the corresponding structures, across a broad range of hydrogen bonded materials. Furthermore, it highlights the need to allow flexible molecules when anharmonic potentials are used in force-field based studies of quantum nuclear effects.

(To appear on Proc. Natl. Acad. Sci.)
Contact person: angelos.michaelides@ucl.ac.uk

Speeding up plane-wave electronic-structure calculations using graphics-processing units

Stefan Maintz, Bernhard Eck, Richard Dronskowski
Institute of Inorganic Chemistry, RWTH Aachen University,
D-52056 Aachen, Germany

Abstract

We report on a source-code modification of the density-functional program suite VASP which benefits from the use of graphics-processing units (GPUs). For the electronic minimization needed to achieve the ground state using an implementation of the blocked Davidson iteration scheme (EDDAV), speed-ups of up to 3.39 on S1070 devices or 6.97 on a C2050 device were observed when calculating an ion-conductor system of actual research interest. Concerning the GPU specialty—memory throughput—the low double-precision performance forms the bottleneck on the S1070, whereas on the Fermi cards the code reaches 61.7% efficiency while not suffering from any accuracy losses compared to well-established calculations performed on a central processing unit (CPU). The algorithmic bottleneck was found to be the multiplication of rectangular matrices. An initial idea to solve this problem is given.

(In press at Computer Physics Communications)
Contact person: drons@HAL9000.ac.rwth-aachen.de

Li/MgO - The Drosophila Catalyst for Methane Oxidative Coupling: A Critical Assessment

Sebastian Arndt[1], Guillaume Laugel[1], Sergey Levchenko[2],
Raimund Horn[2], Manfred Baerns[2], Matthias Scheffler[2],
Robert Schlögl[2], and Reinhard Schomäacker[1]
[1] *Technical University Berlin, Department of Chemistry,*
Strasse des 17 Juni 124, 10623 Berlin, Germany
[2] *Fritz-Haber-Institut der Max-Planck-Gesellschaft,*
Faradayweg 4–6, 14195 Berlin, Germany

Abstract

Li/MgO is one of the most frequently investigated catalysts for the oxidative coupling of methane. Besides catalytic testing, it is also a suitable system to perform surface science experiments and quantum chemical calculations, which is not possible for many other active catalysts. However, the real structure of Li/MgO, the nature of the active center and the structure-activity relationship remain unclear, despite of all the research which has been done. The aim of this review is to summarize the available knowledge on Li/MgO to structure, accelerate and improve the ongoing work on this catalytic system.

(Submitted to: Catal. Rev. Sci. Eng. (2011).)
Contact person: Sergey Levchenko levchenko@fhi-berlin.mpg.de)

Free gold clusters: Beyond the static, mono-structure description

Elizabeth C. Beret, Luca M. Ghiringhelli, and Matthias Scheffler
Fritz-Haber-Institut der Max-Planck-Gesellschaft,
Faradayweg 4–6, 14195 Berlin, Germany

Abstract

The thermodynamical stability of free, pristine gold clusters at finite temperature, and of cluster+ligands complexes at finite temperature and in the presence of an atmosphere composed of O_2 and CO, is studied employing parallel tempering and *ab initio* atomistic thermodynamics. We focus on Au_{13}, which displays a significant fluxional behavior: Even at low temperature (100 K) this cluster exhibits a multitude of structures that dynamically transform into each other. At finite temperature, the preference of this cluster for three-dimensional *versus* planar structures is found to result from entropic effects. For gold clusters containing from one to four gold atoms in an O_2 + CO atmosphere, we apply *ab initio* atomistic thermodynamics. On the basis of these considerations, we single out a likely reaction path for CO oxidation catalyzed by gold clusters.

(Submitted to: Faraday Discussions (2011).)
Contact person: Elizabeth Beret (beret@fhi-berlin.mpg.de)

Activation Energies for Diffusion of Defects in Si: The Role of the Exchange-Correlation Functional

Stefan K. Estreicher[1], Daniel J. Backlund[2],
Christian Carbogno[3], and Matthias Scheffler[3]
[1] *Physics Department, Texas Tech University,*
Lubbock TX 79409-1051, USA
[2] *2Texas Tech University Health Sciences Center,*
IT - Room 1C384, Lubbock TX 79409, USA
[3] *Fritz-Haber-Institut der Max-Planck-Gesellschaft,*
Faradayweg 4–6, 14195 Berlin, Germany

Abstract

The activation energies for diffusion (E_a) of defects in Si are calculated using density-functional theory. The migration paths are obtained from the nudged-elastic band method. The E_a's, calculated with four exchange-correlation functionals (E_xc), are compared to experimental data. The E_a's of 'atomic-like' interstitials are mostly independent of E_xc, but those of strongly bound impurities are sensitive to the choice of E_xc. The most accurate values are systematically obtained with the RPBE form of the generalized gradient approximation. The 'theoretical error bar' associated with the choice of E_xc reflects that the accuracy of the method differs at the minima and saddle points of the potential-energy surfaces.

(Angew. Chem., accepted (2011).)
Contact person: Christian Carbogno (carbogno@fhi-berlin.mpg.de)

Enhanced Dipole Moments in Photo-Excited TTF-TCNQ Dimers

Mina Yoon[1,2], Yoshiyuki Miyamoto[3], and Matthias Scheffler[1]
[1] *Fritz-Haber-Institut der Max-Planck-Gesellschaft,*
Faradayweg 4–6, 14195 Berlin, Germany
[2] *Materials Science and Technology Division,*
Oak Ridge National Laboratory, Oak Ridge, TN 37831-6032, USA
[3] *Green Innovation Research Laboratories,*
NEC Corp., 34 Miyukigaoka, Tsukuba 305-8501, Japan

Abstract

We have studied the dynamics of electron transfer between the molecules of an organic donor-acceptor pair upon absorption of light. Specifically we will consider TTF (Tetrathiafulvalene)- TCNQ (7,7,8,8-tetracyanoquinodimethane) donor-acceptor pair using time-dependent density functional theory with the local-density approximation. The molecular planes of the two components are parallel to each other, and the optical transition probability is found to be highest when the optical electric field (E-field) is parallel to these planes. Under this condition, absorption induces additional electron transfer from TTF to TCNQ in the π-orbitals perpendicular to the molecular plane, and consequently, we find that the dimers dipole moment perpendicular to the molecular axes is enhanced with the increase rate of 1% in 15 fs. This enhancement reflects the fact that photo-excited electron-hole (e-h) pair tends to be separated and move away from each other. We thus suggest potential photovoltaic devices employing these molecules as building blocks.

(Submitted to: Nano Lett. (2010))
Contact person: Mina Yoon (yoon@fhi-berlin.mpg.de)

Semiempirical Rate Constants for Complex Chemical Kinetics: First-Principles Assessment and Rational Refinement

Matteo Maestri[1,3] and Karsten Reuter[2,3]
[1]*Laboratory of Catalysis and Catalytic Processes,*
Dipartimento di Energia, Politecnico di Milano,
Piazza Leonardo da Vinci 32, 20133 Milano, Italy
[2]*Department Chemie, Technische Universität München,*
Lichtenbergstrasse 4, 85747 Garching, Germany
[3]*Fritz-Haber-Institut der Max-Planck-Gesellschaft,*
Faradayweg 4–6, 14195 Berlin, Germany

Abstract

An accurate description of the elementary steps involved in a catalytic process is the basis for a reliable microkinetic modeling of the surface chemistry. Though desirable, a first-principles calculation of the reaction parameters is presently unfeasible but for models involving a small number of reactions. For complex catalytic systems, semiempirical approaches are therefore often employed to estimate reaction barriers and coverage effects. Here, we assess the semiempirical unity bond index quadratic exponential potential (UBI-QEP) scheme, frequently used to estimate activation energies of elementary surface reactions from thermochemical data. Benchmarked against an extensive DFT data set for a range of surface catalytic reactions, the prevalent formulation is found to exhibit large errors with individual barriers deviating by more than 100to the blindness of UBI-QEP with respect to the nature of the involved transition states and to an intrinsic inconsistency in the established parameterization procedure. A simple modification of this procedure that maintains the dependence on bond distances underlying the UBI-QEP idea, but simultaneously recovers the consistency with the reference thermochemistry leads to a significant improvement in the accuracy of the predicted barriers. Insight into the nature of the transition state enters the scheme through one remaining empirical parameter. Such insight is established for many classes of reactions, but can alternatively come from selected first-principles calculations. For the present data set the UBI-QEP barriers provided by the modified scheme fall consistently within a window of +10% around the DFT reference data. At a corresponding uncertainty the semiempirical estimates provide invaluable data for the analysis of complex reaction schemes otherwise not easy to obtain. In particular in conjunction with systematic sensitivity analyses, they might even be the enabling tool for detailed microkinetic modeling approaches to technological systems, most of which are presently outside the capabilities of an exhaustive first-principles treatment. Much beyond the specific UBI-QEP framework our study thus nicely demonstrates the necessity and virtue of a first-principles assessment of prevalent semiempirical approaches in practical catalysis research – in terms of both a reliability assessment and rational refinement.

(Angew. Chem. 123, 1226-1229 (2011).)
Contact person: Matteo Maestri (matteo.maestri@polimi.it)

A reliable first principles approach for calculating phonon spectra in disordered alloys

Oscar Grånäs[2], Biswanath Dutta[1], Subhradip Ghosh[1] and Biplab Sanyal[2]
[1]*Department of Physics, Indian Institute of Technology Guwahati,*
Guwahati, Assam 781039, India
[2]*Department of Physics and Astronomy, Uppsala University,*
Box-516, SE-75120 Uppsala, Sweden

Abstract

The lattice dynamics in substitutional disordered alloys with constituents having large size differences is driven by strong disorder in masses, inter-atomic force constants and local environments. In this letter, a new first-principles approach based on special quasi random structures and itinerant coherent potential approximation to compute the phonon spectra of such alloys is proposed and applied to $\mathrm{Ni}_{0.5}\mathrm{Pt}_{0.5}$ alloy. The agreement between our results with the experiments are found to be much better than previous models of disorder due to an accurate treatment of the interplay of inter-atomic forces among various pairs of chemical specie. This new formalism serves as a potential solution to the longstanding problem of a proper microscopic understanding of lattice dynamical behavior of disordered alloys.

(Submitted to Phys. Rev. Lett)

Contact person: Biswanath Dutta (b.dutta@iitg.ernet.in)

5 SCIENTIFIC HIGHLIGHT OF THE MONTH

First-principles calculations of the Berry curvature of Bloch states for charge and spin transport of electrons

M. Gradhand[1], D.V. Fedorov[2], F. Pientka[2,3], P. Zahn[2], I. Mertig[2,1], and B.L. Györffy[4]

1 - Max-Planck-Institut für Mikrostrukturphysik, Weinberg 2, D-06120 Halle, Germany
2 - Institut für Physik, Martin-Luther-Universität Halle-Wittenberg, D-06099 Halle, Germany
3 - Dahlem Center for Complex Quantum Systems and Fachbereich Physik, Freie Universität Berlin, 14195 Berlin, Germany
4 - H.H.Wills Physics Laboratory, University of Bristol, Bristol BS8 1TH, United Kingdom

Abstract

Recent progress in *wave packet dynamics* based on the insight of M. V. Berry pertaining to adiabatic evolution of quantum systems has led to the need that a new property of a Bloch state, the Berry curvature, has to be calculated from first principles. We report here on the response to this challenge by the *ab initio* community during the past decade. First we give a tutorial introduction of the conceptual developments we mentioned above. Then we describe four methodologies which have been developed for first-principles calculations of the Berry curvature. Finally, in Section 3, to illustrate the significance of the new developments, we report some results of calculations of interesting physical properties like anomalous and spin Hall conductivity.

1 Introduction: Semiclassical electronic transport in solids and wave packet dynamics with the Berry curvature

Some recent, remarkable advances in the semiclassical description of charge and spin transport by electrons in solids motivate a revival of interest in a detailed **k**-point by **k**-point study of their band structure. A good summary of the conceptual developments and the experiments they have stimulated has been given by Di Xiao, Ming-Che Chang and Qian Niu [1]. Here we wish to review only the role and prospects of first-principles electronic structure calculations in this rapidly moving field.

1.1 New features of the Boltzmann equation

Classically, particle transport is considered to take place in phase space whose points are labeled by the position vector **r** and the momentum **p** and described by the distribution function

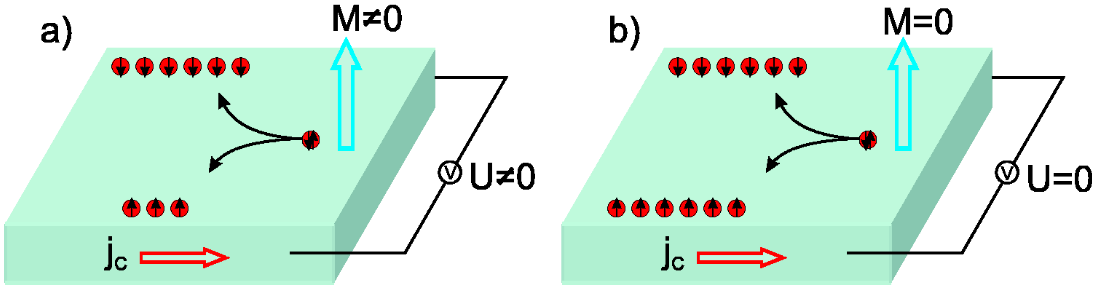

Figure 1: a) The anomalous Hall effect and b) the spin Hall effect.

$f(\mathbf{r},\mathbf{p},\mathrm{t})$ which satisfies the Boltzmann equation. Electrons in solids fit into this framework if we view the particles as wave packets constructed from the Bloch waves, $\Psi_{n\mathbf{k}}(\mathbf{r}) = e^{i\mathbf{k}\cdot\mathbf{r}}u_n(\mathbf{r},\mathbf{k})$, eigenfunctions of the crystal Hamiltonian $\hat{H}$. If such a wave packet is strongly centered at $\mathbf{k}_c$ in the Brillouin zone it predominantly includes Bloch states with quantum numbers $\mathbf{k}$ close to $\mathbf{k}_c$ and the particle can be said to have a momentum $\hbar\,\mathbf{k}_c$. Then, if we call its spatial center $\mathbf{r}_c$ its position, the transport of electrons can be described by an ensemble of such quasiparticles. One of these is described with the distribution function $f_n(\mathbf{r}_c,\mathbf{k}_c,\mathrm{t})$. For simplicity the band index n is dropped in the following. As $f(\mathbf{r}_c,\mathbf{k}_c,\mathrm{t})$ evolves in phase space the usual form of the Boltzmann equation, which preserves the total probability, is given by

$$\partial_t f + \dot{\mathbf{r}}_c\cdot\boldsymbol{\nabla}_{\mathbf{r}_c} f + \dot{\mathbf{k}}_c\cdot\boldsymbol{\nabla}_{\mathbf{k}_c} f = \left(\frac{\delta f}{\delta t}\right)_{\mathrm{scatt}} \quad . \tag{1}$$

Here the first term on the left hand side is the derivative with respect to the explicit time dependence of f, the next two terms account for the time dependence of $\mathbf{r}_c$ and $\mathbf{k}_c$, and the term on the right hand side is due to scattering of electron states, by defects and other perturbations *in* and *out* of the considered phase space volume centered at $\mathbf{r}_c$ and $\mathbf{k}_c$. The time evolution of $\mathbf{r}_c\,(\mathrm{t})$ and $\mathbf{k}_c\,(\mathrm{t})$ is given by semiclassical equations of motion which in the presence of external electric $\mathbf{E}$ and magnetic $\mathbf{B}$ fields take conventionally the following form

$$\dot{\mathbf{r}}_c = \frac{1}{\hbar}\frac{\partial\mathcal{E}_{n\mathbf{k}}}{\partial\mathbf{k}}\bigg|_{\mathbf{k}=\mathbf{k}_c} = \mathbf{v}_n(\mathbf{k}_c)\ , \tag{2}$$

$$\hbar\dot{\mathbf{k}}_c = -e\mathbf{E} - e\dot{\mathbf{r}}_c\times\mathbf{B}\ . \tag{3}$$

Here, the group velocity $\mathbf{v}_n(\mathbf{k}_c)$ involves the unperturbed band structure. In the presence of a constant electric $\mathbf{E} = (E_x,0,0)$ and magnetic $\mathbf{B} = (0,0,B_z)$ field the solution of the above equations yields the Hall resistivity $\rho_{xy} \propto B_z$. However, for a ferromagnet with magnetization $\mathbf{M} = (0,0,M_z)$ the above theory can not account for the experimentally observed (additional) *anomalous* contribution $\rho_{xy} \propto M_z$. For a necessary correction of the theory, one needs to construct a wave packet

$$\mathrm{W}_{\mathbf{k}_c,\mathbf{r}_c}(\mathbf{r},t) = \sum_{\mathbf{k}} a_{\mathbf{k}}(\mathbf{k}_c,t)\Psi_{n\mathbf{k}}(\mathbf{r}) \tag{4}$$

carefully taking into account the phase of the weighting function $a_{\mathbf{k}}(\mathbf{k}_c,t)$. Requiring the wave packet to be centered at $\mathbf{r}_c = \langle W_{\mathbf{k}_c,\mathbf{r}_c}|\mathbf{r}|W_{\mathbf{k}_c,\mathbf{r}_c}\rangle$, it follows that $a_{\mathbf{k}}(\mathbf{k}_c,t) = |a_{\mathbf{k}}(\mathbf{k}_c,t)|\,e^{i(\mathbf{k}-\mathbf{k}_c)\cdot\mathbf{A}_n(\mathbf{k}_c)}$, where

$$\mathbf{A}_n\,(\mathbf{k}_c) = i\int_{\mathrm{u.c.}} \mathrm{d}^3\mathrm{r}\ u_n^*(\mathbf{r},\mathbf{k}_c)\boldsymbol{\nabla}_{\mathbf{k}}u_n(\mathbf{r},\mathbf{k}_c) \tag{5}$$

is the Berry *connection* as will be discussed in detail in the next Section. Note that the integral is restricted to only one unit cell (u.c.).

Now, using the wave packet of Eq. (4), one can construct the Lagrangian

$$L(t) = \langle W| \, i\hbar\partial_t - \hat{H} \, |W\rangle \ , \tag{6}$$

and minimize the action functional $\mathrm{S}[\mathbf{r}_c(t), \mathbf{k}_c(t)] = \int^{t} dt' L(t')$ with respect to arbitrary variations in $\mathbf{r}_c(t)$ and $\mathbf{k}_c(t)$. This manoeuvre replaces the quantum mechanical expectation values with respect to $\mathrm{W}_{\mathbf{k}_c,\mathbf{r}_c}(\mathbf{r},t)$ by the classical equations of motion for $\mathbf{r}_c(t)$ and $\mathbf{k}_c(t)$. From the Euler-Lagrange equations

$$\partial_t \frac{\partial L}{\partial \dot{\mathbf{k}}_c} - \frac{\partial L}{\partial \mathbf{k}_c} = 0 \ \text{ and } \ \partial_t \frac{\partial L}{\partial \dot{\mathbf{r}}_c} - \frac{\partial L}{\partial \mathbf{r}_c} = 0 \ , \tag{7}$$

one gets

$$\begin{aligned} \dot{\mathbf{r}}_c &= \frac{1}{\hbar} \frac{\partial \mathcal{E}_{n\mathbf{k}}}{\partial \mathbf{k}} \bigg|_{\mathbf{k}=\mathbf{k}_c} - \dot{\mathbf{k}}_c \times \mathbf{\Omega}_n\left(\mathbf{k}_c\right) \ , &(8)\\ \hbar\dot{\mathbf{k}}_c &= -e\mathbf{E} - e\dot{\mathbf{r}}_c \times \mathbf{B} \ . &(9)\end{aligned}$$

Here $\mathbf{\Omega}_n(\mathbf{k}_c)$ is the so-called Berry *curvature*, defined as

$$\mathbf{\Omega}_n(\mathbf{k}_c) = \mathbf{\nabla}_{\mathbf{k}} \times \mathbf{A}_n(\mathbf{k})|_{\mathbf{k}=\mathbf{k}_c} \ , \tag{10}$$

the main subject of this Highlight.

In comparison to Eq. (2), the new equation of motion for $\mathbf{r}_c(t)$ given by Eq. (8) has an additional term proportional to the electric field called the anomalous velocity

$$\mathbf{v}_n^a(\mathbf{k}_c) = \frac{e}{\hbar}\mathbf{E} \times \mathbf{\Omega}_n\left(\mathbf{k}_c\right) \ . \tag{11}$$

The presence of this velocity provides the anomalous contribution to the Hall current $j_y^H = j_y^{H,\uparrow} + j_y^{H,\downarrow}$, where the spin-resolved currents may be written as

$$\begin{aligned} j_y^{H,\uparrow} &= -e \int\limits_{BZ} \frac{\mathrm{d}^3\mathrm{k}_c}{(2\pi)^3} \, \dot{r}^{y}_{c\uparrow}(\mathbf{k}_c) f_\uparrow\left(\mathbf{k}_c\right) = \sigma^{\uparrow}_{yx}\left(M_z\right) E_x \ . &(12)\\ j_y^{H,\downarrow} &= -e \int\limits_{BZ} \frac{\mathrm{d}^3\mathrm{k}_c}{(2\pi)^3} \, \dot{r}^{y}_{c\downarrow}(\mathbf{k}_c) f_\downarrow\left(\mathbf{k}_c\right) = \sigma^{\downarrow}_{yx}\left(M_z\right) E_x \ . &(13)\end{aligned}$$

In that notation $f_\uparrow\left(\mathbf{k}_c\right)$ and $f_\downarrow\left(\mathbf{k}_c\right)$ are the spin-resolved distribution functions which are solutions of Eq. (1). In the limit of no scattering they reduce to the equilibrium distribution functions and only the intrinsic mechanism governed by the anomalous velocity of Eq. (11) contributes to the Hall component. In general, $j_y^{H,\uparrow}$ and $j_y^{H,\downarrow}$ have opposite sign because of $\dot{\mathbf{r}}_c(\mathbf{k}_c)$. However, the resulting charge current is non-vanishing (see Fig. 1 (a)) due to the fact, that the number of spin-up and spin-down electrons differs in ferromagnets with a finite magnetization $\mathbf{M} \neq 0$. In contrast to the AHE in ferromagnets, the absence of the magnetization in normal metals leads to the presence of time inversion symmetry and, as a consequence, $j_y^{H,\uparrow} = -j_y^{H,\downarrow}$. This provides a vanishing charge current, i.e. Hall voltage, but the existence of a pure spin current as depicted in Fig. 1 (b), which is known as the spin Hall effect (SHE).

1.2 Berry phase, connection and curvature of Bloch electrons

Here we introduce shortly the concept of such relatively novel quantities as the Berry phase, connection, and curvature which arise in case of an adiabatic evolution of a system.

1.2.1 Adiabatic evolution of eigenstates

Let us consider an eigenvalue problem of the following form

$$\widehat{H}(\mathbf{r}, \lambda_1, \lambda_2, \lambda_3)\Phi_n(\mathbf{r}; \lambda_1, \lambda_2, \lambda_3) = \mathcal{E}_n(\lambda_1, \lambda_2, \lambda_3)\Phi_n(\mathbf{r}; \lambda_1, \lambda_2, \lambda_3) \ , \tag{14}$$

where $\widehat{H}$ is a differential operator, Φ_n and $\mathcal{E}_n$ are the nth eigenfunction and eigenvalue, respectively, the vector $\mathbf{r}$ is a variable, and λ_1, λ_2, λ_3 are parameters restricted for simplicity to the number of three. A mathematical problem of general interest is the way such eigenfunctions change if the set $\boldsymbol{\lambda} = (\lambda_1, \lambda_2, \lambda_3)$ changes slowly with time. If it is assumed that the process is adiabatic, that is to say there is no transition from one to another state, then for long it was argued that a state $\Phi_n(t = 0)$ evolves in time as $\Phi_n(t) = \Phi_n(t = 0)$ $\exp\left(-\frac{i}{\hbar}\int\limits_0^t dt'\mathcal{E}_n(\lambda_1(t'), \lambda_2(t'), \lambda_3(t')) + i\gamma_n(t)\right)$, where the phase $\gamma_n(t)$ is meaningless as it can be 'gauged' away. In 1984 M. V. Berry [2] has discovered that while this is true for an arbitrary open path in the parameter space, for a path that returns to the starting values $\lambda_1(0)$, $\lambda_2(0)$, and $\lambda_3(0)$ the accumulated phase is 'gauge' invariant and is therefore a meaningful and measurable quantity. In particular, he showed that for a closed path, labeled C in Fig. 2, the phase γ_n can be described by a line integral as

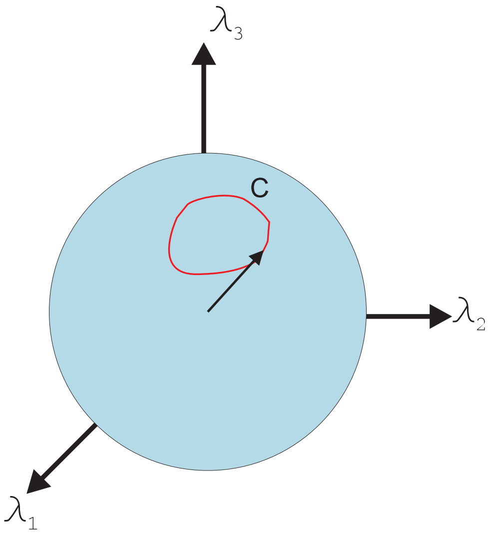

Figure 2: A closed path in the parameter space.

$$\gamma_n = \oint_C \mathrm{d}\boldsymbol{\lambda} \cdot \mathbf{A}_n(\boldsymbol{\lambda}) \ , \tag{15}$$

where the connection $\mathbf{A}_n(\boldsymbol{\lambda})$ is given by

$$\mathbf{A}_n(\boldsymbol{\lambda}) = i \int \mathrm{d}^3\mathrm{r} \ \Phi_n^*(\mathbf{r}, \boldsymbol{\lambda})\boldsymbol{\nabla}_{\boldsymbol{\lambda}}\Phi_n(\mathbf{r}, \boldsymbol{\lambda}) \ . \tag{16}$$

The surprise is that although the connection is not 'gauge' invariant, γ_n and even more interestingly the curvature

$$\mathbf{\Omega}_n(\boldsymbol{\lambda}) = \boldsymbol{\nabla}_{\boldsymbol{\lambda}} \times \mathbf{A}_n(\boldsymbol{\lambda}) \tag{17}$$

are. As will be shown presently, these ideas are directly relevant for the dynamics of wave packets in the transport theory discussed above.

1.2.2 Berry connection and curvature for Bloch states

Somewhat surprisingly the above discussion has a number of interesting things to say about the wave packets in the semiclassical approach for spin and charge transport of electrons in crystals. Its relevance becomes evident if we take the Schrödinger equation for the Bloch state

$$\left(-\frac{\hbar^2}{2m}\boldsymbol{\nabla}_{\mathbf{r}}^2 + V(\mathbf{r})\right)\Psi_{n\mathbf{k}}(\mathbf{r}) = \mathcal{E}_{n\mathbf{k}}\Psi_{n\mathbf{k}}(\mathbf{r}) \ , \tag{18}$$

and rewrite it for the periodic part of the Bloch function

$$\left(-\frac{\hbar^2}{2m}\left(\boldsymbol{\nabla}_{\mathbf{r}} + i\mathbf{k}\right)^2 + V(\mathbf{r})\right)u_n(\mathbf{r},\mathbf{k}) = \mathcal{E}_{n\mathbf{k}}u_n(\mathbf{r},\mathbf{k}) \ . \tag{19}$$

The point is that the differential equation for $\Psi_{n\mathbf{k}}(\mathbf{r})$, a simultaneous eigenfunction of the translation operator and the Hamiltonian, does not depend on the wave vector, since $\mathbf{k}$ only labels the eigenvalues of the translation operator. However, in Eq. (19) $\mathbf{k}$ appears as a parameter and hence the above discussion of the Berry phase, the corresponding connection, and curvature applies directly. In short, for each band n there is a connection associated with every $\mathbf{k}$ given by

$$\mathbf{A}_n(\mathbf{k}) = i\int\limits_{\text{u.c.}} \mathrm{d}^3\mathrm{r}\ u_n^*(\mathbf{r},\mathbf{k})\boldsymbol{\nabla}_{\mathbf{k}}u_n(\mathbf{r},\mathbf{k}) \ . \tag{20}$$

Furthermore, the curvature

$$\mathbf{\Omega}_n(\mathbf{k}) = \boldsymbol{\nabla}_{\mathbf{k}} \times \mathbf{A}_n(\mathbf{k}) = i\int\limits_{\text{u.c.}} \mathrm{d}^3\mathrm{r}\boldsymbol{\nabla}_{\mathbf{k}}u_n^*(\mathbf{r},\mathbf{k}) \times \boldsymbol{\nabla}_{\mathbf{k}}u_n(\mathbf{r},\mathbf{k}) \tag{21}$$

is the quantity that appears in the semiclassical equation of motion for the wave packet in Eq. (8). Thus, the curvature and the corresponding anomalous velocity in Eq. (11) associated with the band n are properties of $u_n(\mathbf{r},\mathbf{k})$. To emphasize this point, we note that the Bloch functions $\Psi_{n\mathbf{k}}(\mathbf{r})$ are orthogonal to each other

$$\langle\Psi_{n\mathbf{k}}|\Psi_{n'\mathbf{k}'}\rangle = \int\limits_{\text{crystal}} \mathrm{d}^3\mathrm{r}\ \Psi_{n\mathbf{k}}^*(\mathbf{r})\Psi_{n'\mathbf{k}'}(\mathbf{r}) = \delta_{\mathbf{k},\mathbf{k}'}\delta_{n,n'} \ , \tag{22}$$

and hence $\mathbf{k}$ is not a parameter. In contrast, $u_n(\mathbf{r},\mathbf{k})$ is orthogonal to $u_{n'}(\mathbf{r},\mathbf{k})$ but not to $u_n(\mathbf{r},\mathbf{k}')$ as this is an eigenfunction of a different Hamiltonian.

The observation that the above connection and curvature are properties of the periodic part of the Bloch function prompts a further comment. Note, that for vanishing periodic potential the Bloch functions would reduce to plane waves. Constructing the wave packet from plane waves means $u_n(\mathbf{r},\mathbf{k}) = 1$. Evidently, this means that $\mathbf{\Omega}_n(\mathbf{k})$ and $\mathbf{A}_n(\mathbf{k})$ are zero and this fact is consistent with the general notion that the connection and the curvature arise from including only one or in any case finite number of bands, in constructing the wave packet. The point is that the neglected bands are the 'outside world' referred to in the original article of M. V. Berry [2]. In contrast the expansion in terms of plane waves does not neglect any bands since there is just one band. Thus, the physical origin of the connection and the curvature is due to the periodic crystal potential breaking up the full spectrum of the parabolic free particle dispersion relation into bands, usually separated by gaps, and we select states only from a limited number of such bands to represent the wave packet.

1.3 Abelian and non-Abelian curvatures

So far we have introduced the Berry connection and curvature for a non-degenerate band. In case of degenerate bands the conventional adiabatic theorem fails. In the semiclassical framework a correct treatment incorporates a wave packet constructed from the degenerate bands [3, 4]. As a consequence, the Berry curvature must be extended to a tensor definition in analogy to non-Abelian gauge theories. This extension is originally due to Wilczek and Zee [5].

Let us consider the eigenspace $\{|u_i(\mathbf{k})\rangle : \ i \in \Sigma\}$ of some N-fold degenerate eigenvalue. For Bloch states the elements of the non-Abelian Berry connection $\bar{\bar{\mathbf{A}}}(\mathbf{k})$ read

$$\mathbf{A}_{ij}(\mathbf{k}) = i\,\langle u_i(\mathbf{k})\,|\,\boldsymbol{\nabla}_{\mathbf{k}} u_j(\mathbf{k})\rangle \qquad i,j \in \Sigma\ , \tag{23}$$

where $\Sigma = \{1, ..., N\}$ contains all indices of the degenerate subspace. The definition of the curvature tensor $\bar{\bar{\boldsymbol{\Omega}}}(\mathbf{k})$ in a non-Abelian gauge theory has to be extended by substituting the curl with the covariant derivative as

$$\begin{aligned} \bar{\bar{\boldsymbol{\Omega}}}(\mathbf{k}) &= \boldsymbol{\nabla}_{\mathbf{k}} \times \bar{\bar{\mathbf{A}}}(\mathbf{k}) - i\bar{\bar{\mathbf{A}}}(\mathbf{k}) \times \bar{\bar{\mathbf{A}}}(\mathbf{k})\ , \\ \boldsymbol{\Omega}_{ij}(\mathbf{k}) &= i\left\langle \frac{\partial u_i(\mathbf{k})}{\partial \mathbf{k}} \right| \times \left| \frac{\partial u_j(\mathbf{k})}{\partial \mathbf{k}} \right\rangle + i \sum_{l\in\Sigma} \left\langle u_i(\mathbf{k}) \left| \frac{\partial u_l(\mathbf{k})}{\partial \mathbf{k}} \right.\right\rangle \times \left\langle u_l(\mathbf{k}) \left| \frac{\partial u_j(\mathbf{k})}{\partial \mathbf{k}} \right.\right\rangle . \end{aligned} \tag{24}$$

The subspace of degenerate eigenstates is subject to a U(N) gauge freedom and observables should be invariant with respect to a gauge transformation of the basis set

$$\left\{ \sum_i U_{ij}(\mathbf{k})\,|u_i(\mathbf{k})\rangle \ :\ i \in \Sigma \right\} \qquad \text{with } \bar{\bar{U}}(\mathbf{k}) \in \mathrm{U}(N). \tag{25}$$

Consequently, the Berry connection and curvature are transformed according to

$$\bar{\bar{\mathbf{A}}}'(\mathbf{k}) = \bar{\bar{U}}^{\dagger}(\mathbf{k})\bar{\bar{\mathbf{A}}}(\mathbf{k})\bar{\bar{U}}(\mathbf{k}) + i\bar{\bar{U}}^{\dagger}(\mathbf{k})\boldsymbol{\nabla}_{\mathbf{k}}\bar{\bar{U}}(\mathbf{k})\ , \tag{26}$$

$$\bar{\bar{\boldsymbol{\Omega}}}'(\mathbf{k}) = \bar{\bar{U}}^{\dagger}(\mathbf{k})\bar{\bar{\boldsymbol{\Omega}}}(\mathbf{k})\bar{\bar{U}}(\mathbf{k}). \tag{27}$$

The curvature is now a *covariant* tensor and thus not directly observable. However, there are gauge invariant quantities that may be derived from it. From gauge theories it is known that the connection and the curvature must lie in the tangent space of the gauge group U(N), i.e., the Lie algebra $\mathfrak{u}(N)$. The above definition of the Lie algebra differs by an unimportant factor of i from the mathematical convention.

The most prominent example of a non-Abelian Berry curvature appears in materials with time-reversal (T) and inversion (I) symmetry. For each $\mathbf{k}$ point there exist two orthogonal states $|\Psi_{n\uparrow\mathbf{k}}\rangle$ and $|\Psi_{n\downarrow\mathbf{k}}\rangle = \mathrm{TI}\,|\Psi_{n\uparrow\mathbf{k}}\rangle$ with the same energy, the Kramers doublet. In general, a choice for $|\Psi_{n\uparrow\mathbf{k}}\rangle$ determines the second basis state $|\Psi_{n\downarrow\mathbf{k}}\rangle$ only up to a phase. However, the symmetry transformation fixes the phase relationship between both basis states. This reduces the gauge freedom to SU(2) and, consequently, the Berry connection will be an $\mathfrak{su}(2)$ matrix, which means its trace vanishes. This is verified easily

$$\begin{aligned}\langle u_{n\downarrow}(\mathbf{k})|\boldsymbol{\nabla}_{\mathbf{k}} u_{n\downarrow}(\mathbf{k})\rangle &= \langle \mathrm{TI}\, u_{n\uparrow}(\mathbf{k})|\boldsymbol{\nabla}_{\mathbf{k}} \mathrm{TI}\, u_{n\uparrow}(\mathbf{k})\rangle = \langle \mathrm{TI}\, u_{n\uparrow}(\mathbf{k})|\mathrm{TI}\, \boldsymbol{\nabla}_{\mathbf{k}} u_{n\uparrow}(\mathbf{k})\rangle \\ &= -\,\langle u_{n\uparrow}(\mathbf{k})|\boldsymbol{\nabla}_{\mathbf{k}} u_{n\uparrow}(\mathbf{k})\rangle \ .\end{aligned} \tag{28}$$

For the Kramers doublet the Berry curvature must always be an $\mathfrak{su}(2)$ matrix because a gauge transformation induces a unitary transformation of the curvature which does not alter the trace. The symmetry analysis in the next Section has to be altered since time reversal also changes the spin $\mathrm{TI}\,\boldsymbol{\Omega}_{n\uparrow\uparrow}(\mathbf{k}) = -\boldsymbol{\Omega}_{n\uparrow\uparrow}(\mathbf{k}) = \boldsymbol{\Omega}_{n\downarrow\downarrow}(\mathbf{k})$, which proves that the trace is indeed zero. Therefore, in contrast to the spinless case, the Berry curvature may be nontrivial even in nonmagnetic materials with inversion symmetry.

Despite the Berry curvature being gauge covariant we may derive several observables from it. As we have seen the trace of the Berry curvature is gauge invariant. In the multiband formulation of the semiclassical theory, the expectation value of the curvature matrix with respect to the spinor amplitudes enters the equations of motion [3,4]. In the context of the spin Hall effect one is interested in $\mathrm{Tr}(\bar{\bar{S}}_j\bar{\bar{\Omega}}_i)$, where $\bar{\bar{S}}_j$ is the j-th component of the vector valued $\mathfrak{su}(2)$ spin matrix.

1.4 Symmetry, Topology, Codimension and the Dirac monopole

It is expedient to exploit symmetries for the evaluation of the Berry curvature. From Eqs. (20) and (21) we may easily determine the behavior of $\boldsymbol{\Omega}_n(\mathbf{k})$ under symmetry operations. In crystals with a center of inversion, the corresponding symmetry operation leaves $\mathcal{E}_{n\mathbf{k}}$ invariant while $\mathbf{r}$, $\dot{\mathbf{r}}$, $\mathbf{k}$, and $\dot{\mathbf{k}}$ change sign, and hence $\boldsymbol{\Omega}_n(\mathbf{k}) = \boldsymbol{\Omega}_n(-\mathbf{k})$. On the other hand, when time-reversal symmetry is present $\mathcal{E}_{n\mathbf{k}}$, $\mathbf{r}$, and $\dot{\mathbf{k}}$ remain unchanged while $\dot{\mathbf{r}}$ and $\mathbf{k}$ are inverted, which leads to an antisymmetric Berry curvature $\boldsymbol{\Omega}_n(\mathbf{k}) = -\boldsymbol{\Omega}_n(-\mathbf{k})$. Thus, if time-reversal and inversion symmetry are present simultaneously the Berry curvature vanishes identically. This is true in spinless materials only. Taking into account spin we have to acknowledge the presence of a twofold degeneracy of all bands throughout the Brillouin zone [6, 7], the Kramers doublet, discussed in the previous Section.

As was mentioned already in Section 1.2.2, the Berry curvature of a band arises due to the projection onto this band, e.g., in the semiclassical one band theory it keeps an information about the influence of other adjacent bands. If a band is well separated from all other bands by an energy scale large compared to one set by the time scale of the adiabatic evolution, the influence of the other bands is negligible. In contrast, degeneracies of energy bands deserve special attention, since the conventional adiabatic theorem fails there. Special attention has been paid to pointlike degeneracies, where the intersection of two energy bands is shaped like a double cone or a diabolo (Fig. 3, left). These degeneracies are called diabolical points [8].

According to M. V. Berry [2] we can linearize the Hamiltonian near such a point and rewrite it as an effective two band Hamiltonian

$$H(\mathbf{r}) = \begin{pmatrix} z & x-iy \\ x+iy & -z \end{pmatrix} = r_i\sigma_i \ , \tag{29}$$

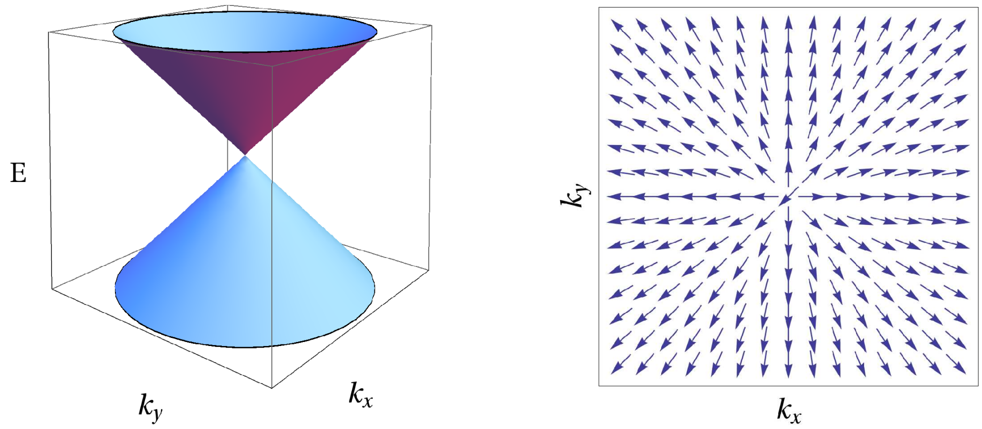

Figure 3: Left: Conical intersection of energy surfaces. Right: Direction of the Monopole field.

where σ_i are the Pauli matrices and the $\mathbf{r}$ space is some suitable parametrization of the Brillouin zone. The eigenvalues are $\pm|\mathbf{r}|$, hence the dispersion is shaped like a cone. The degeneracy lies at the origin of the $\mathbf{r}$ parameter space and the curvature is given by

$$\boldsymbol{\Omega}_{\pm}(\mathbf{r}) = \pm\frac{1}{2}\frac{\mathbf{r}}{r^3} \ . \tag{30}$$

This is precisely the form of the monopole of a magnetic field with a charge 1/2 (Fig. 3, right). Diabolical points always have this charge, while nonlinear intersections may have higher charges [10]. In general, the monopole charge is a topological invariant and quantized to integer multiples of 1/2. This is a consequence of the quantization of the Dirac monopole [9].
In more general language, the Berry curvature flux through a closed two-dimensional manifold ∂M is the first Chern number C_n of that manifold and thus an integer. Since the (Abelian) curvature is defined as the curl of the connection it must be divergence free except for the monopoles. We can then exploit Gauss' theorem

$$C_n = \frac{1}{2\pi}\int_{\partial M} \mathrm{d}\sigma\, \boldsymbol{\Omega}_n \mathbf{n} = \frac{1}{2\pi}\int_{M} \mathrm{d}^3\mathrm{r}\ \boldsymbol{\nabla}\cdot\boldsymbol{\Omega}_n = m \ , \qquad m \in \mathbb{N} \ . \tag{31}$$

Here $\mathbf{n}$ is the normal vector of the surface element. If we assume that each monopole contributes a Chern number of ±1 the above equation implies for the Berry curvature $\boldsymbol{\nabla}\cdot\boldsymbol{\Omega} = 4\pi\sum_j g_j\delta(\mathbf{r}-\mathbf{r}_j)$, where $g_j = \pm1/2$. The solution of this differential equation yields the source term of the Berry curvature

$$\boldsymbol{\Omega}(\mathbf{r}) = \sum_j g_j \frac{\mathbf{r}-\mathbf{r}_j}{|\mathbf{r}-\mathbf{r}_j|^3} + \boldsymbol{\nabla}\times\mathbf{A}(\mathbf{r}) \ , \tag{32}$$

which proves that there are monopoles with a charge quantized to 1/2 times an integer.
The mathematical interpretation of the Berry curvature in terms of the theory of fiber bundles and Chern classes and the connection to the theory of the quantum Hall effect, where the Chern number appears as the Thouless-Kohmoto-Nightingale-den Nijs (TKNN) integer [11] has been first noticed by Simon [12].
However, monopoles are not only interesting in a mathematical sense but also for actual calculations of quantities such as the anomalous Hall conductivity. On the one hand, singularities of the Berry curvature near the Fermi surface greatly influence the numerical stability of the

result. On the other hand, Haldane [13] has pointed out that the Chern number and thus the anomalous Hall conductivity can be changed by creation and annihilation of Berry curvature monopoles.

To identify monopoles in a parameter space one is interested in degeneracies that do not occur on account of any symmetry and have thus been called accidental. For a single Hamiltonian without symmetries the occurrence of degeneracies in the discrete spectrum is infinitely unlikely. For Hamiltonians that depend on a set of parameters one can ask how many parameters are needed in order to encounter a twofold degenerate eigenvalue. This number is called codimension. According to a theorem by von Neumann and Wigner [14], for a generic Hamiltonian the answer is three. In other words, degeneracies are points in a three-dimensional parameter space like the Brillouin zone. For this reason accidental degeneracies are diabolical points.

If the Hamiltonian is *real*, which is equivalent to being invariant with respect to time reversal, the number of parameters we have to vary reduces to two [15]. However, we have seen that in the case of nonmagnetic crystals with inversion symmetry each band is twofold degenerate. This degeneracy arises due to a symmetry and is not accidental. The theorem of von Neumann and Wigner does not apply. As a consequence, *accidental* degeneracies of two different bands would have to be fourfold. In this case the codimension is five and the occurrence of an accidental degeneracy is infinitely unlikely in the Brillouin zone.

This is the reason why we only observe avoided crossings for nonmagnetic crystals with inversion symmetry, since and all accidental crossings are lifted by spin-orbit coupling. In order to encounter accidental two-fold degeneracies of codimension two, we would, thus, need to consider a nonmagnetic band structure without inversion symmetry of the lattice.

1.5 The spin polarization gauge

As was discussed in the previous Sections, in spinless crystals with time-reversal and inversion symmetry the Berry curvature vanishes at every $\mathbf{k}$ point [16]. If spin degrees of freedom are taken into account the band structure is twofold degenerate throughout the Brillouin zone due to Kramers degeneracy plus inversion symmetry and consequently the Berry curvature is represented by an element of the Lie algebra $\mathfrak{su}(2)$. In contrast to the scalar case, this matrix is gauge covariant and hence not observable. In order to gain some insight to the Berry curvature of nonmagnetic materials we would like to visualize it. To this end we must be able to compare the Berry curvature at different points in $\mathbf{k}$ space, thus we have to choose a universal gauge. Then we can plot the first diagonal element of the $\mathfrak{su}(2)$ matrix which should be continuous in such a gauge.

One natural choice of a gauge (let us call it gauge I) is to ensure that the spin polarization of one Kramers state is always parallel to the z direction *and* positive [17] that is

$$\begin{aligned}\langle\Psi_{\uparrow\mathbf{k}}|\sigma_x|\Psi_{\uparrow\mathbf{k}}\rangle &= 0\\ \langle\Psi_{\uparrow\mathbf{k}}|\sigma_y|\Psi_{\uparrow\mathbf{k}}\rangle &= 0.\\ \langle\Psi_{\uparrow\mathbf{k}}|\sigma_z|\Psi_{\uparrow\mathbf{k}}\rangle &> 0\end{aligned} \tag{33}$$

This means for the second Kramers state

$$\langle\Psi_{\downarrow\mathbf{k}}|\sigma_z|\Psi_{\downarrow\mathbf{k}}\rangle = -\langle\Psi_{\uparrow\mathbf{k}}|\sigma_z|\psi_{\uparrow\mathbf{k}}\rangle < 0. \tag{34}$$

More generally, we will discuss the spin polarization as an $\mathfrak{su}(2)$ matrix $\langle\boldsymbol{\sigma}\rangle$, as it appears in the context of the spin Hall effect, whose first diagonal element is aligned along the z direction in this gauge. The positiveness is essential, since in this way we can distinguish the two degenerate states. However, this fails when the spin polarization goes to zero within this gauge.

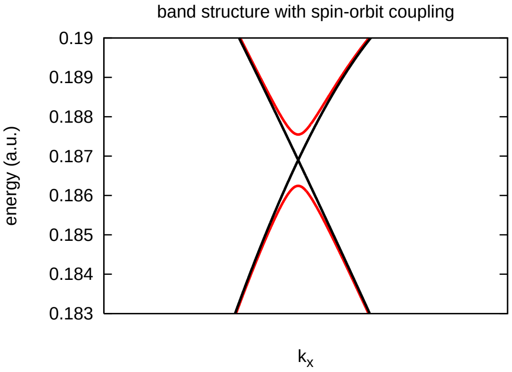

Figure 4: Spin-orbit coupling lifts an accidental degeneracy of the nonmagnetic band structure.

As a result of the theorem by Wigner and von Neumann [14] discussed in Section 1.4, we do not expect accidental degeneracies in nonmagnetic materials, since they are lifted by spin-orbit coupling. When two bands get close at some point in the Brillouin zone they "repel" each other depending on the strength of spin-orbit coupling. The lifting of accidental degeneracies by spin-orbit coupling, at a certain point S in momentum space, is illustrated in Fig. 4, where the band structure with (without) spin-orbit interaction is displayed in red (black). Similar to real crossings in the magnetic case, there are peaks of the Berry curvature at these points, since the two degenerate bands under consideration are significantly influenced by the neighboring bands. However, in contrast to the magnetic case, the curvature remains finite.

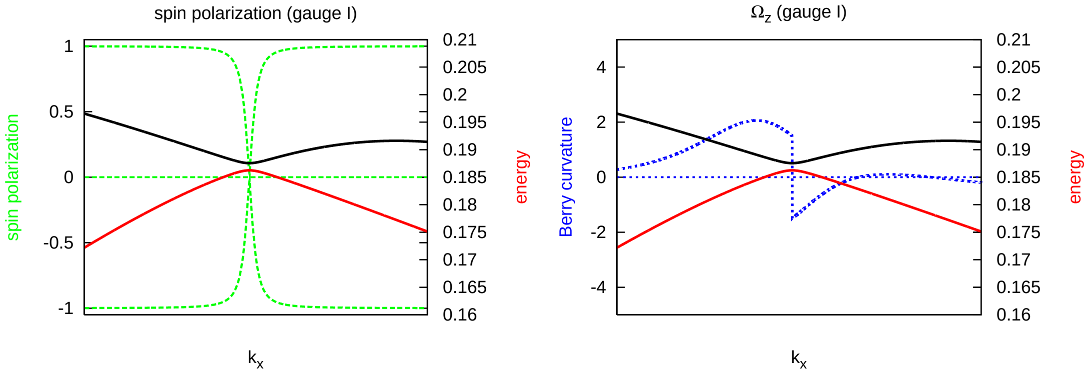

Figure 5: Left: First diagonal element of the $\mathfrak{su}(2)$ spin polarization (green) of the Kramers doublet in gauge I. Right: The first diagonal element of the $\mathfrak{su}(2)$ Berry curvature (blue) jumps in gauge I.

When introducing gauge I, we remarked that it is necessary to enforce a positive sign of $\langle\Psi_{\uparrow\mathbf{k}}|\sigma_z|\Psi_{\uparrow\mathbf{k}}\rangle$ in addition to the alignment of the spin polarization along the z axis. By doing this one can distinguish the two degenerate Kramers states $|\Psi_{\uparrow\mathbf{k}}\rangle$ and $|\Psi_{\downarrow\mathbf{k}}\rangle$ according to their spin polarization. This criterion becomes useless once there is a point where the spin polarization vanishes in the gauge chosen. This is exactly the case when the avoided crossing originates from a degeneracy lifted by spin-orbit coupling.

This situation is illustrated in Fig. 5, where the spin polarization for both Kramers states of the lower doublet is shown. The spin polarization becomes zero at the avoided crossing. In fact, the picture suggests that the spin polarizations of both states change sign, which means that by enforcing gauge I we have changed from the first to the second Kramers state while crossing point S. Indeed, this is verified by the graph of the first diagonal element of the Berry curvature in this gauge presented in Fig. 5. Exactly at the point where the spin polarization vanishes, the Berry curvature changes sign, jumping from one degenerate state to the other. This jumping is unsatisfactory, since it does not allow us to plot the Berry curvature consistently throughout the BZ without adjustment by hand. A way out is provided by a different gauge [18, 19].

This new gauge (let us call it gauge II) describes the nonmagnetic crystal as the limit of vanishing exchange splitting in a magnetic crystal. The task is then to find the unitary transformation that diagonalizes the perturbation operator H_{xc} in the degenerate subspace of the Kramers doublet. This amounts to the condition

$$\langle \Psi_{\uparrow\mathbf{k}} | \mathcal{H}_{\mathrm{xc}} | \Psi_{\downarrow\mathbf{k}} \rangle \sim \langle \Psi_{\uparrow\mathbf{k}} | \sigma_z | \Psi_{\downarrow\mathbf{k}} \rangle = 0, \tag{35}$$

where $\Psi_{\uparrow\downarrow\mathbf{k}}$ denote the two Kramers states. The above equation accounts for the two free parameters we have to fix. Furthermore, we choose the sign as

$$\langle \Psi_{\uparrow\mathbf{k}} | \sigma_z | \Psi_{\uparrow\mathbf{k}} \rangle > 0. \tag{36}$$

In gauge II the diagonal elements of the nonmagnetic spin polarization represents the analytical continuation of the magnetic spin polarizations with vanishing exchange splitting.

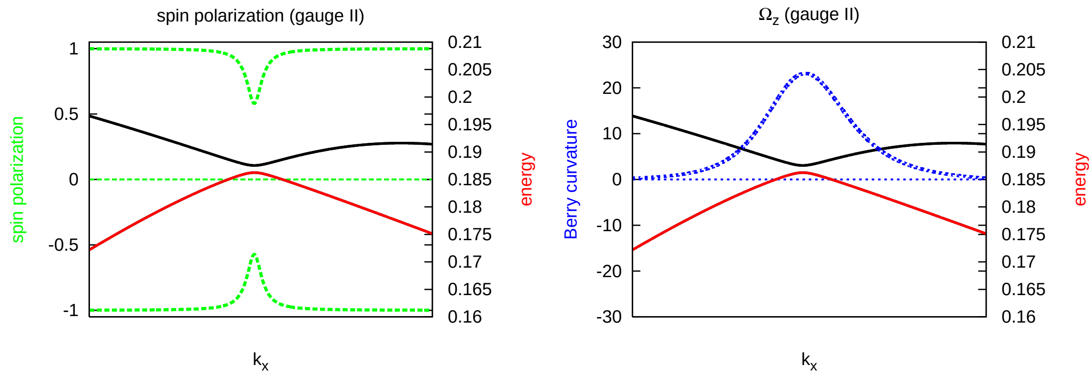

Figure 6: Left: Nonmagnetic spin polarization (green) of the lower doublet in gauge II. Right: The first diagonal element of the $\mathfrak{su}(2)$ Berry curvature (blue) remaining continuous in gauge II.

In Fig. 6 the same avoided crossing as in Fig. 5 is shown while gauge II has been imposed. The spin polarization now remains finite and the Berry curvature is continuous, thus we have resolved the ambiguity.

2 First principle calculations of the Berry curvature for Bloch Electrons

2.1 KKR method

In this Section we describe the most recent of four methods developed for calculating the Berry curvature. This approach [20] is based on the screened version of the venerable KKR method [21] and is motivated by the fact that in the multiple scattering theory the wave vector $\mathbf{k}$ enters the problem only through the structure constants $G^s_{QQ'}(\mathcal{E};\mathbf{k})$, defined in Eq. (40). Those depend on the geometrical arrangement of the scatterers but not on the scattering potentials at the lattice sites. Hence the sort of $\mathbf{k}$ derivatives that occur in the definition of the connection in Eq. (20) should involve only the derivative $\boldsymbol{\nabla}_{\mathbf{k}} G^s_{QQ'}(\mathcal{E};\mathbf{k})$ easy to calculate within the screened KKR method. In what follows we demonstrate that such expectation can indeed be realized and an efficient algorithm is readily constructed which takes full advantage of these features.

As it is clear from Eqs. (20) and (21), the connection $\mathbf{A}_n(\mathbf{k})$ and the curvature $\boldsymbol{\Omega}_n(\mathbf{k})$ are the properties of the periodic component $u_n(\mathbf{r},\mathbf{k})$ of the Bloch state $\Psi_{n\mathbf{k}}(\mathbf{r})$. However, as in most band theory methods, in the KKR one calculates the Bloch wave. Thus, to facilitate the calculation of $\mathbf{A}_n(\mathbf{k})$ and $\boldsymbol{\Omega}_n(\mathbf{k})$ from $\Psi_{n\mathbf{k}}(\mathbf{r})$ one must recast the problem. A useful way to proceed with it is to rewrite

$$\begin{aligned}\mathbf{A}_n(\mathbf{k}) &= i\int\limits_{\text{u.c.}} \mathrm{d}^3\mathrm{r}\; u_n^\dagger(\mathbf{r},\mathbf{k})\boldsymbol{\nabla}_{\mathbf{k}} u_n(\mathbf{r},\mathbf{k}) \\ &= i\int\limits_{\text{u.c.}} \mathrm{d}^3\mathrm{r}\; \Psi^*_{n\mathbf{k}}(\mathbf{r})\boldsymbol{\nabla}_{\mathbf{k}}\Psi_{n\mathbf{k}}(\mathbf{r}) + \int\limits_{\text{u.c.}} \mathrm{d}^3\mathrm{r}\; \Psi^*_{n\mathbf{k}}(\mathbf{r})\mathbf{r}\Psi_{n\mathbf{k}}(\mathbf{r})\;, \end{aligned} \tag{37}$$

where the integrals are over the unit cell.

Since the most interesting physical consequences of the Berry curvature occur in spin-orbit coupled systems, the theory is developed in terms of a fully relativistic multiple scattering theory based on the Dirac equation. In short, the four component Dirac Bloch wave [22] is expanded around one site in terms of the local scattering solutions $\Phi_Q(\mathcal{E};\mathbf{r})$ of the radial Dirac equation as [20]

$$\Psi_{n\mathbf{k}}(\mathbf{r}) = \sum_Q C_{n,Q}(\mathbf{k})\Phi_Q(\mathcal{E};\mathbf{r})\;. \tag{38}$$

In such a representation the expansion coefficients $C_{n,Q}(\mathbf{k})$ are solutions of the eigenvalue problem

$$\bar{\bar{M}}(\mathcal{E};\mathbf{k})\bar{C}_n(\mathbf{k}) = \lambda_n\bar{C}_n(\mathbf{k}) \quad \text{with} \quad \bar{C}_n(\mathbf{k}) = \{C_{n,Q}(\mathbf{k})\} \tag{39}$$

for the KKR matrix [20]

$$M_{QQ'}(\mathcal{E};\mathbf{k}) = G^s_{QQ'}(\mathcal{E};\mathbf{k})\Delta t^s_{Q'}(\mathcal{E}) - \delta_{QQ'}\;, \tag{40}$$

where $G^s_{QQ'}(\mathcal{E};\mathbf{k})$ are the relativistic screened structure constants, $\Delta t^s_{Q'}(\mathcal{E})$ is the Δt matrix of the reference system [21] and the eigenvalues $\lambda_n(\mathcal{E},\mathbf{k})$ vanish for $\mathcal{E} = \mathcal{E}_{n\mathbf{k}}$.

Note, that the eigenvalue problem Eq. (39) depends parametrically on $\mathbf{k}$. Therefore, one can formally deploy the original arguments of M. V. Berry [2] to derive an expression for the curvature associated with this problem. Namely, one finds (here for the sake of simplicity we assume the matrix $\bar{\bar{M}}$ to be Hermitian) [20]

$$\boldsymbol{\Omega}_n^{\mathrm{KKR}}(\mathbf{k}) = -Im\{\sum_{m\neq n} \tfrac{\bar{C}_n^\dagger \boldsymbol{\nabla}_{\mathbf{k}} \bar{\bar{M}} \bar{C}_m \times \bar{C}_m^\dagger \boldsymbol{\nabla}_{\mathbf{k}} \bar{\bar{M}} \bar{C}_n}{(\lambda_n-\lambda_m)^2}\} \; . \tag{41}$$

Evidently, this curvature is the property of the KKR matrix $\bar{\bar{M}}(\mathcal{E};\mathbf{k})$. What is important about this result is the fact that the $\mathbf{k}$ derivative operates only on $\bar{\bar{M}}(\mathcal{E};\mathbf{k})$ and therefore it can be expressed simply by

$$\partial\bar{\bar{G}}^s(\mathcal{E};\mathbf{k})/\partial\mathbf{k} = i\sum_{\mathbf{R}} \mathbf{R} e^{i\mathbf{kR}} \bar{\bar{G}}^s(\mathcal{E};\mathbf{R}) \; , \tag{42}$$

due to the feature of the screened structure constants. This formula can be easily evaluated since the screened real space structure constants $\bar{\bar{G}}^s(\mathcal{E};\mathbf{R})$ are short ranged. While this is reassuringly consistent with the expectation at the beginning of this Section this is not the whole story. The curvature of the KKR matrix is not that of the Hamiltonian

$$\hat{H}_{\mathbf{k}}(\mathbf{r}) = e^{-i\mathbf{k}\cdot\mathbf{r}} \hat{H}(\mathbf{r}) e^{i\mathbf{k}\cdot\mathbf{r}} \tag{43}$$

whose eigenfunctions are the periodic components $u_n(\mathbf{r},\mathbf{k})$. In fact, when we evaluate Eq. (37) we find

$$\mathbf{A}_n(\mathbf{k}) = \mathbf{A}_n^k(\mathbf{k}) + \mathbf{A}_n^r(\mathbf{k}) = \mathbf{A}_n^{\mathrm{KKR}}(\mathbf{k}) + \mathbf{A}_n^v(\mathbf{k}) + \mathbf{A}_n^r(\mathbf{k}) \; . \tag{44}$$

Here we have the KKR part

$$\mathbf{A}_n^{\mathrm{KKR}}(\mathbf{k}) = i\bar{C}_n^\dagger \boldsymbol{\nabla}_{\mathbf{k}} \bar{C}_n = -\mathrm{Im}\{\bar{C}_n^\dagger \boldsymbol{\nabla}_{\mathbf{k}} \bar{C}_n\} \; , \tag{45}$$

$$\mathbf{A}_n^v(\mathbf{k}) = i\mathbf{v}_n \bar{C}_n^\dagger \bar{\bar{\Delta}} \bar{C}_n = -\mathbf{v}_n \mathrm{Im}\{\bar{C}_n^\dagger \bar{\bar{\Delta}} \bar{C}_n\} \; , \tag{46}$$

with

$$(\bar{\bar{\Delta}})_{QQ'}(\mathcal{E}) = \delta_{QQ'} \int_{\mathrm{u.c.}} \mathrm{d}^3\mathrm{r}\; \Phi_Q^\dagger(\mathcal{E};\mathbf{r}) \tfrac{\partial\Phi_{Q'}(\mathcal{E};\mathbf{r})}{\partial\mathcal{E}} \; , \tag{47}$$

and the dipole part

$$\mathbf{A}_n^r(\mathbf{k}) = \bar{C}_n^\dagger(\mathbf{k}) \bar{\bar{\mathbf{r}}} \bar{C}_n(\mathbf{k}) \; , \tag{48}$$

with the matrix elements of the position operator

$$(\bar{\bar{\mathbf{r}}})_{QQ'}(\mathcal{E}) = \int_{\mathrm{u.c.}} \mathrm{d}^3\mathrm{r}\; \Phi_Q^\dagger(\mathcal{E};\mathbf{r}) \mathbf{r} \Phi_{Q'}(\mathcal{E};\mathbf{r}) \; . \tag{49}$$

As will be shown, the contribution from the first term of r.h.s of Eq. (44) provides the curvature associated with the KKR matrix in Eq. (41), while the velocity term $\mathbf{A}_n^v(\mathbf{k})$ and dipole term $\mathbf{A}_n^r(\mathbf{k})$ lead to small corrections.

2.1.1 KKR formula for the Abelian Berry curvature

Starting from the Berry connection introduced above it is straightforward to extend the method to the Berry curvature expressions. For the Abelian case the Berry curvature is given by three contributions

$$\boldsymbol{\Omega}_n(\mathbf{k}) = \boldsymbol{\nabla}_{\mathbf{k}} \times \mathbf{A}_n(\mathbf{k}) = \boldsymbol{\Omega}_n^k(\mathbf{k}) + \boldsymbol{\Omega}_n^r(\mathbf{k}) = \boldsymbol{\Omega}_n^{\mathrm{KKR}}(\mathbf{k}) + \boldsymbol{\Omega}_n^v(\mathbf{k}) + \boldsymbol{\Omega}_n^r(\mathbf{k}) \; , \tag{50}$$

stemming from the analogue terms in Eq. (44). Here, the KKR part which is shown to be the dominant contribution [20] takes the simple form

$$\mathbf{\Omega}_n^{\mathrm{KKR}}(\mathbf{k}) = i\boldsymbol{\nabla}_{\mathbf{k}}\bar{C}_n^{\dagger} \times \boldsymbol{\nabla}_{\mathbf{k}}\bar{C}_n = -\mathrm{Im}\{\boldsymbol{\nabla}_{\mathbf{k}}\bar{C}_n^{\dagger} \times \boldsymbol{\nabla}_{\mathbf{k}}\bar{C}_n\}\ , \tag{51}$$

where just the expansion coefficients are involved. Now, an important step is to shift the $\mathbf{k}$ derivative towards the $\mathbf{k}$-dependent KKR matrix. Actually, because of the chosen KKR-basis set in Eq. (38), one has to deal with a non-Hermitian KKR matrix. However, in order to simplify the further discussion and to have a clear insight into the presented approach, here the matrix $\bar{\bar{M}}$ is assumed to be Hermitian. Then, introducing a complete set of eigenvectors of the KKR matrix leads to Eq. (41) which is quite similar to one obtained in the original paper of M. V. Berry. The difference is just that the $\mathbf{k}$-dependent Hamiltonian is replaced by the $\mathbf{k}$-dependent KKR matrix of finite dimension. As was already discussed, the partial $\mathbf{k}$ derivative of the KKR matrix can be calculated analytically within the screened KKR method. In a similar way the velocity and the dipole terms can be treated. Both contributions are typically one order of magnitude smaller than the KKR part [20]. Moreover, the velocity part of the Berry curvature is always strictly perpendicular to the group velocity. This fact is a technically very important feature since for a Fermi surface integral over the Berry curvature this contribution would identically vanish.

2.1.2 KKR formula for non-Abelian Berry curvature

For a treatment of the non-Abelian Berry curvature not only the conventional connection has to be taken into account, but also the commutator, which is provided by the requirement of the gauge invariant theory, has to be considered. As a consequence, the Berry curvature is defined as

$$\mathbf{\Omega}_{ij}(\mathbf{k}) = i\left\langle \boldsymbol{\nabla}_{\mathbf{k}} u_i\left(\mathbf{k}\right)\right| \times \left|\boldsymbol{\nabla}_{\mathbf{k}} u_j\left(\mathbf{k}\right)\right\rangle - i\sum_{l\in\Sigma}\left\langle \boldsymbol{\nabla}_{\mathbf{k}} u_i\left(\mathbf{k}\right)\middle| u_l\left(\mathbf{k}\right)\right\rangle \times \left\langle u_l\left(\mathbf{k}\right)\middle|\boldsymbol{\nabla}_{\mathbf{k}} u_j\left(\mathbf{k}\right)\right\rangle . \tag{52}$$

Here, as was discussed in section 1.3, Σ contains all indices of the degenerate subspace. Rewriting it in terms of the Bloch states yields

$$\begin{aligned}\mathbf{\Omega}_{ij}(\mathbf{k}) &= i\left\langle \boldsymbol{\nabla}_{\mathbf{k}}\Psi_{i\mathbf{k}}\right| \times \left|\boldsymbol{\nabla}_{\mathbf{k}}\Psi_{j\mathbf{k}}\right\rangle + \left\langle \boldsymbol{\nabla}_{\mathbf{k}}\Psi_{i\mathbf{k}} \times \mathbf{r}\middle|\Psi_{j\mathbf{k}}\right\rangle - \left\langle \Psi_{i\mathbf{k}}\middle|\mathbf{r} \times \boldsymbol{\nabla}_{\mathbf{k}}\Psi_{j\mathbf{k}}\right\rangle - \\ &- \sum_{l\in\Sigma}\{i\left\langle \boldsymbol{\nabla}_{\mathbf{k}}\Psi_{i\mathbf{k}}\middle|\Psi_{l\mathbf{k}}\right\rangle \times \left\langle \Psi_{l\mathbf{k}}\middle|\boldsymbol{\nabla}_{\mathbf{k}}\Psi_{j\mathbf{k}}\right\rangle - \left\langle \Psi_{i\mathbf{k}}\middle|\mathbf{r}\middle|\Psi_{l\mathbf{k}}\right\rangle \times \left\langle \Psi_{l\mathbf{k}}\middle|\boldsymbol{\nabla}_{\mathbf{k}}\Psi_{j\mathbf{k}}\right\rangle + \\ &+ \left\langle \boldsymbol{\nabla}_{\mathbf{k}}\Psi_{i\mathbf{k}}\middle|\Psi_{l\mathbf{k}}\right\rangle \times \left\langle \Psi_{l\mathbf{k}}\middle|\mathbf{r}\middle|\Psi_{j\mathbf{k}}\right\rangle + i\left\langle \Psi_{i\mathbf{k}}\middle|\mathbf{r}\middle|\Psi_{l\mathbf{k}}\right\rangle \times \left\langle \Psi_{l\mathbf{k}}\middle|\mathbf{r}\middle|\Psi_{j\mathbf{k}}\right\rangle\}\ ,\end{aligned} \tag{53}$$

and a similar decomposition into the KKR, velocity and dipole parts

$$\mathbf{\Omega}_{ij}(\mathbf{k}) = \mathbf{\Omega}_{ij}^{\mathrm{KKR}}(\mathbf{k}) + \mathbf{\Omega}_{ij}^{v}(\mathbf{k}) + \mathbf{\Omega}_{ij}^{r}(\mathbf{k}) \tag{54}$$

can be performed.

In Fig. 7 the absolute value of the diagonal component of the non-Abelian (vector-valued matrix) Berry curvature over the Fermi surface of several metals is shown. An evident anisotropy of the distribution with the values enhanced in z direction is caused by the choice of the gauge

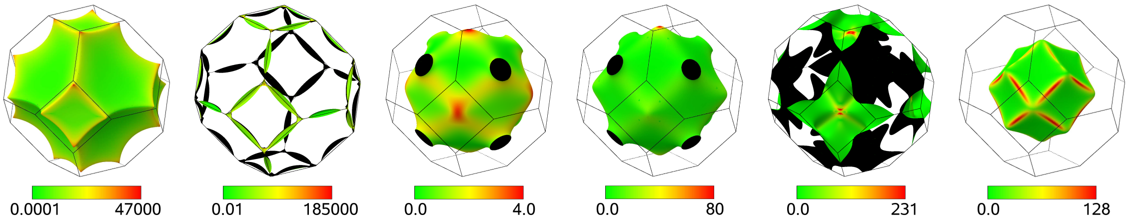

Figure 7: The absolute value (in a.u.) of the diagonal component of the non-Abelian Berry curvature $|\Omega^z_{ii}(\mathbf{k})|$ for the Fermi surface of several metals. From left to right Al (3rd and 5th band), Cu (11th band), Au (11th band) and Pt (9th and 11th band). For Al we used a logarithmic scale to visualize the important regions [20].

transformation, namely the requirement for the off-diagonal matrix elements of the spin operator $\Sigma_z = \beta\sigma_z$ in the subspace of the two degenerate bands to be zero (see the discussion in Section 1.5). In addition, near degeneracies at the Fermi level lead to enhanced Berry curvatures as can be seen for Al and Pt. Furthermore, the energy resolved Berry curvature (here $S(\mathcal{E})$ is the isosurface of constant energy $\mathcal{E}$ in the $\mathbf{k}$ space)

$$\Omega^z(\mathcal{E}) = \sum_n \int_{S(\mathcal{E})} \frac{d^2k}{|v^n(\mathbf{k})|} \Omega^{z,+}_n(\mathbf{k}) \tag{55}$$

is shown in Fig. 8. It proves that the KKR part of Eq. 54 is the dominant contribution to the Berry curvature. Clearly visible is the quite spiky structure of the curvature as a function of the energy. As discussed in the literature, this makes the integration of the Berry curvature computationally demanding, requiring a large number of $\mathbf{k}$ and energy points.

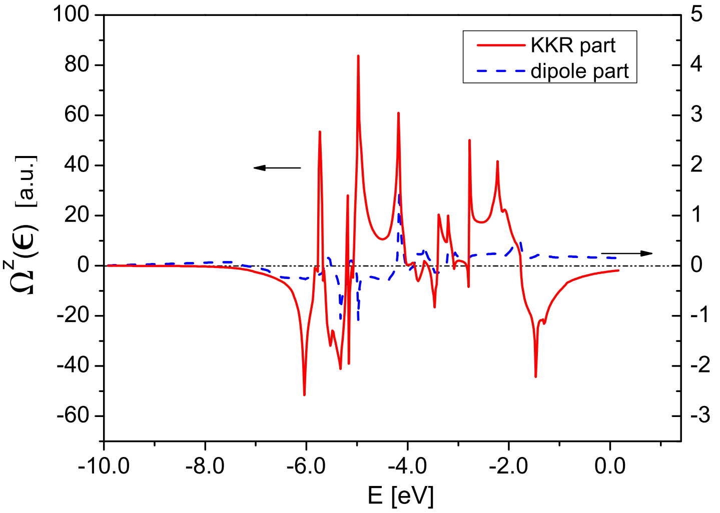

Figure 8: The energy resolved Berry curvature $\Omega^z(\mathcal{E})$ for Au divided into the parts $\Omega^{\mathrm{KKR}}(\mathcal{E})$ and $\Omega^r(\mathcal{E})$ according to Eq. 54 and [20].

2.2 Tight-Binding Model

The tight-binding model provides a convenient framework for studying the geometric quantities in band theory. We will briefly introduce the tight-binding method with spin-orbit coupling and exchange interaction. The usefulness of this model is then illustrated by discussing interesting features of the Berry curvature of a simple band structure.

The tight-binding model assumes that the electronic wave function at each lattice site is well localized around the position of the atom. For this purpose one assumes the crystal potential to consist of a sum of spherically symmetric, somewhat strongly attractive potentials located at the core positions. The idea is to treat the overlap matrix elements as a perturbation and consequently expand the wave function in a basis of atomic orbitals $\{\phi_\alpha(\mathbf{r}-\mathbf{R}_i)\}$. The ansatz

$$\Psi_{n\mathbf{k}}(\mathbf{r}) = \frac{1}{\sqrt{N}} \sum_{\mathbf{R}_i} e^{i\mathbf{k}\mathbf{R}_i} \sum_{\alpha} C_{n\alpha}(\mathbf{k}) \phi_\alpha(\mathbf{r}-\mathbf{R}_i) \tag{56}$$

ensures that $\Psi_{n\mathbf{k}}$ fulfills the Bloch theorem. The simplest case involves neglecting the overlap matrix elements of the wave function

$$\langle \phi_\beta(\mathbf{r}-\mathbf{R}_j) \,|\, \phi_\alpha(\mathbf{r}-\mathbf{R}_i) \rangle \sim \delta_{\alpha,\beta} \delta_{\mathbf{R}_i,\mathbf{R}_j} . \tag{57}$$

The normalized eigenfunctions in on-site approximation are subject to the eigenvalue problem $\langle \Psi_{n\mathbf{k}} | H | \Psi_{n\mathbf{k}} \rangle = \mathcal{E}_{n\mathbf{k}}$. The solution to this problem in the tight-binding formulation of Eq. (56) requires the diagonalization of the tight-binding matrix

$$H_{\alpha\beta} = \sum_{\mathbf{R}_i,\mathbf{R}_j} e^{i\mathbf{k}(\mathbf{R}_i-\mathbf{R}_j)} \langle \phi_\alpha(\mathbf{r}-\mathbf{R}_j) | H | \phi_\beta(\mathbf{r}-\mathbf{R}_i) \rangle \ . \tag{58}$$

Then the coefficients $C_{n\alpha}$ are obtained as the components of the eigenvector of this matrix and thus the eigenstates necessary for the evaluation of the Berry curvature are easily accessible.

The matrix elements in Eq. (58) can be parametrized by the method of Slater and Koster [23]. In order to observe a nontrivial Berry curvature we need to take into account spin degrees of freedom. This doubles the number of bands compared to the spinless case. Within the scope of the tight-binding model the spin-orbit interaction is treated as a perturbation

$$V_{\mathrm{SOC}} = \frac{\hbar}{4m^2c^2} \left(\boldsymbol{\nabla}_{\mathbf{r}} V(\mathbf{r}) \times \mathbf{p} \right) \mathbf{S} = V_{\mathrm{SOC}} = \frac{2\lambda}{\hbar^2} \mathbf{L}\mathbf{S} \tag{59}$$

to the Hamiltonian. Here a spherical symmetric potential is assumed and the parameter λ is considered to be small with respect to the on-site and hopping energies. The matrix elements of this operator have been listed elsewhere for basis states of p, d and f symmetry [24] in on-site approximation, although the formalism presented here does not require this approximation.

Furthermore, one can use this model to describe a ferromagnetic material by incorporating an exchange interaction term. The simplest formulation originates from the mean field theory. Without taking into account any temperature dependence, a constant exchange field is assumed and the z axis is chosen as the quantization direction

$$H_{\mathrm{xc}} = -\mathbf{V}_{\mathrm{xc}} \boldsymbol{\sigma} = -V_{\mathrm{xc}} \sigma_z \ , \tag{60}$$

where V_{xc} is a positive real number.

2.2.1 Berry Curvature in the Tight-Binding Model

As in the case of the KKR method discussed in the previous Section, solving the eigenproblem of the tight-binding matrix gives the Bloch wave $|\Psi_{n\mathbf{k}}\rangle$ instead of the periodic function $|u_n(\mathbf{k})\rangle$.

Hence, one also needs to consider the two parts, $\boldsymbol{\Omega}^k(\mathbf{k})$ and $\boldsymbol{\Omega}^r(\mathbf{k})$, of the Berry curvature introduced by Eq. (50). Exploiting the on-site approximation of Eq. (57) and the normalization condition for the coefficents, one gets the first term for the Abelian case in a well known form

$$\begin{aligned}\boldsymbol{\Omega}^k_n(\mathbf{k}) &= i\,\langle \boldsymbol{\nabla}_{\mathbf{k}}\Psi_{n\mathbf{k}}\,|\times|\,\boldsymbol{\nabla}_{\mathbf{k}}\Psi_{n\mathbf{k}}\rangle_{\text{u.c.}} = i\boldsymbol{\nabla}_{\mathbf{k}}\overline{C}^\dagger_n(\mathbf{k})\times\boldsymbol{\nabla}_{\mathbf{k}}\overline{C}_n(\mathbf{k})\\ &= -\mathrm{Im}\sum_{m\neq n}\frac{\overline{C}^\dagger_n(\mathbf{k})\boldsymbol{\nabla}_{\mathbf{k}}\bar{\bar{H}}(\mathbf{k})\overline{C}_m(\mathbf{k})\times\overline{C}^\dagger_m(\mathbf{k})\boldsymbol{\nabla}_{\mathbf{k}}\bar{\bar{H}}(\mathbf{k})\overline{C}_n(\mathbf{k})}{(\mathcal{E}_n-\mathcal{E}_m)^2}\;.\end{aligned}\tag{61}$$

The second, dipole, term is given by

$$\begin{aligned}\boldsymbol{\Omega}^r_n(\mathbf{k}) &= \boldsymbol{\nabla}_{\mathbf{k}}\times\langle\Psi_{n\mathbf{k}}\,|\,\mathbf{r}\,|\,\Psi_{n\mathbf{k}}\rangle_{\text{cell}} = \boldsymbol{\nabla}_{\mathbf{k}}\times\left(\overline{C}^\dagger_n(\mathbf{k})\bar{\bar{\mathbf{r}}}\,\overline{C}_n(\mathbf{k})\right)\\ &= \sum_{m\neq n}2\,\mathrm{Re}\left[\frac{\overline{C}^\dagger_n(\mathbf{k})\boldsymbol{\nabla}_{\mathbf{k}}\bar{\bar{H}}(\mathbf{k})\overline{C}_m(\mathbf{k})}{\mathcal{E}_n-\mathcal{E}_m}\times\left(\overline{C}^\dagger_m(\mathbf{k})\bar{\bar{\mathbf{r}}}\,\overline{C}_n(\mathbf{k})\right)\right]\;,\end{aligned}\tag{62}$$

where we have introduced the vector valued matrix $\bar{\bar{\mathbf{r}}}$ with the components $\mathbf{r}_{\alpha\beta} = \langle\phi_\beta(\mathbf{r})\,|\,\mathbf{r}\,|\,\phi_\alpha(\mathbf{r})\rangle$. Similar to the screened KKR method, the $\mathbf{k}$ derivative of $\bar{\bar{H}}(\mathbf{k})$ in the equations above may be performed analytically and no numerical derivative is needed.

In the case of degenerate bands, the non-Abelian Berry curvature $\boldsymbol{\Omega}_{ij}(\mathbf{k}) = \boldsymbol{\Omega}^k_{ij}(\mathbf{k}) + \boldsymbol{\Omega}^r_{ij}(\mathbf{k})$ is expressed in the following terms (according to Section 1.3, Σ contains all indices of the degenerate subspace)

$$\boldsymbol{\Omega}^k_{ij} = i\sum_{m\notin\Sigma}\frac{\overline{C}^\dagger_i(\mathbf{k})\boldsymbol{\nabla}_{\mathbf{k}}\bar{\bar{H}}(\mathbf{k})\overline{C}_m(\mathbf{k})\times\overline{C}^\dagger_m(\mathbf{k})\boldsymbol{\nabla}_{\mathbf{k}}\bar{\bar{H}}(\mathbf{k})\overline{C}_j(\mathbf{k})}{(\mathcal{E}_i-\mathcal{E}_m)\,(\mathcal{E}_j-\mathcal{E}_m)}\;,\tag{63}$$

$$\begin{aligned}\boldsymbol{\Omega}^r_{ij} = \sum_{m\notin\Sigma}\Bigg[&-\left(\overline{C}^\dagger_i(\mathbf{k})\bar{\bar{\mathbf{r}}}\,\overline{C}_m(\mathbf{k})\right)\times\frac{\overline{C}^\dagger_m(\mathbf{k})\boldsymbol{\nabla}_{\mathbf{k}}\bar{\bar{H}}(\mathbf{k})\overline{C}_j(\mathbf{k})}{\mathcal{E}_j-\mathcal{E}_m}\\ &+\frac{\overline{C}^\dagger_i(\mathbf{k})\boldsymbol{\nabla}_{\mathbf{k}}\bar{\bar{H}}(\mathbf{k})\overline{C}_m(\mathbf{k})}{\mathcal{E}_i-\mathcal{E}_m}\times\left(\overline{C}^\dagger_m(\mathbf{k})\bar{\bar{\mathbf{r}}}\,\overline{C}_j(\mathbf{k})\right)\Bigg]\\ &-i\sum_{l\in\Sigma}\left(\overline{C}^\dagger_i(\mathbf{k})\bar{\bar{\mathbf{r}}}\,\overline{C}_l(\mathbf{k})\right)\times\left(\overline{C}^\dagger_l(\mathbf{k})\bar{\bar{\mathbf{r}}}\,\overline{C}_j(\mathbf{k})\right)\;.\end{aligned}\tag{64}$$

Here only the last term is not a direct generalization of the Abelian Berry curvature. Again it is possible to circumvent the numerical derivative by a summation over all states that do not belong to the degenerate subspace. The last term does not involve any derivative, therefore the sum runs only over the degenerate bands.

2.2.2 Diabolical Points

To illustrate the behavior of the Berry curvature near degeneracies, we present calculations of a simple band structure using the tight-binding method. We consider a ferromagnetic simple cubic crystal with eight bands including one band with s symmetry and three bands with p symmetry for each spin direction. Due to the exchange interaction there is no time-reversal symmetry and the codimension of degeneracies is three.

Regions of the parameter space with a higher symmetry (e.g., high symmetry lines in the Brillouin zone) are more likely to support accidental degeneracies because the symmetry possibly reduces the codimension only in this region. Level crossings on a high symmetry line in the

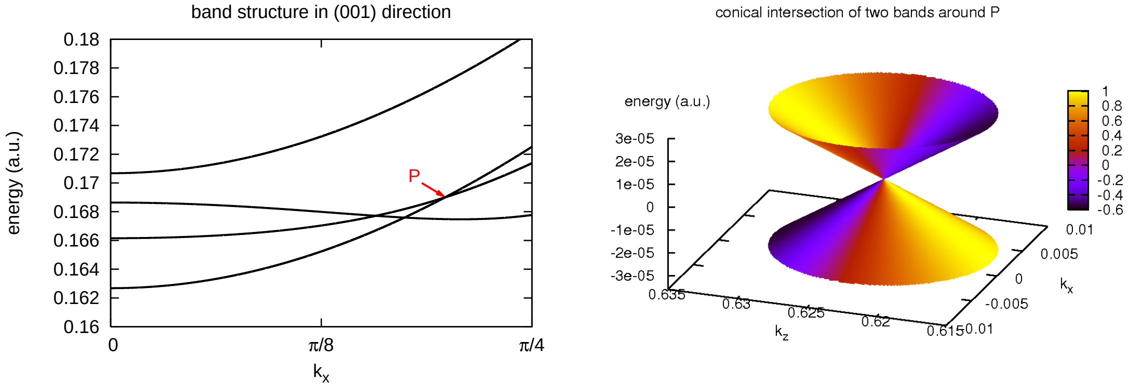

Figure 9: Left: The crossing of some p bands of a ferromagnetic simple cubic band structure near the center of the Brillouin zone. Right: Conical intersection of energy surfaces. The z axis represents the energy dispersion of two intersecting bands over an arbitrary plane in $\mathbf{k}$ space through the diabolical point. The color scale denotes the spin polarization corresponding to each band.

Brillouin zone do not necessarily occur on account of symmetry as long as the bands are not degenerate at points nearby which have the same symmetry.

As an example, in Fig. 9 a few bands of the band structure near the Γ point along a high symmetry line are plotted. There occur three crossings between different bands. On the right-hand side, the energy dispersion in a plane through the degeneracy is displayed in order to show the cone shape of the intersection. The color scale represents the spin polarization $\langle\Psi|\sigma_z|\Psi\rangle$ of the corresponding band. Within one band the spin polarization rapidly changes in the vicinity of the degeneracy. At the degeneracy itself it jumps due to the cusp of the corresponding band. However, when passing the intersection along a straight line in $\mathbf{k}$ space and jumping from the lower to the upper band apparently the spin polarization does not change at all. This is a clear indication that the character of the two bands is exchanged at the intersection.

The behavior of the spin polarization near the diabolical point illustrates how observables are influenced by other bands nearby. The Berry curvature can be viewed as a measure of this coupling which becomes evident from Eqs. (61) and (62), where a sum over all other bands is performed weighted by the inverse energy difference. M. V. Berry has called this in a more general context the coupling to the "rest of the universe" [2]. Hence, the Berry curvature of a single Bloch band generally arises due to a projection onto this band and it becomes large when other bands are close. As we have seen before, a degeneracy produces a singularity of the Berry curvature and the adiabatic single-band approximation fails.

In our case the origin of the Berry curvature is the spin-orbit coupling. Since degenerate or almost degenerate points in the band structure produce large spin mixing of the involved bands, a peak in the Berry curvature can also be understood from this point of view.

As discussed in Section 1.4, we would expect the curvature around the degeneracy to obey the $1/|\mathbf{k}-\mathbf{k}_0|^2$-law of a Coulomb field. The asymptotic, spherically symmetric behavior becomes evident when plotting $1/\sqrt{|\mathbf{\Omega}|}$ in some plane the degeneracy lies in (see Fig. 10). We observe an absolute value function $|\mathbf{k}-\mathbf{k_0}|$, which proves that the Berry curvature really has the form of the monopole field strength given by Eq. (30).

Besides the absolute value we can also examine the direction of the Berry curvature vector. In

Fig. 11, we recognize the characteristic monopole field. In the lower band the monopole is a source, in the upper band a drain of the Berry curvature. This has been expected because a monopole in one band has to be matched by a monopole of opposite charge in the other band involved in the degeneracy.

In general, we may assign a “charge” g to the monopole as in Eq. (30). This charge is quantized to be either integer or half integer. In order to determine the charge numerically one could perform a fit of the numerical data with the monopole field strength. However there is no reason to believe that all directions in $\mathbf{k}$ space must be equivalent. Some distortion in a certain direction might result in ellipsoidal isosurfaces of $|\boldsymbol{\Omega}|$ instead of spherical ones. A different approach, independent from the coordinate system exploits Eq. (31)

$$\int_V \mathrm{d}^3\mathbf{k}\, \boldsymbol{\nabla} \cdot \boldsymbol{\Omega} = \int_{\partial V} \mathrm{d}s \mathbf{n} \cdot \boldsymbol{\Omega} = 2\pi m \qquad m \in \mathbb{Z}, \tag{65}$$

where $\mathbf{n}$ is a normal vector on the bounding surface ∂V of some arbitray volume V. Performing the numerical surface integration causes no problem since the Berry curvature is analytical on the surface unlike at the degeneracy.

So as to validate this formula, the total monopole charge in a sphere of radius r centered at a generic point in the Brillouin zone near P (see Fig. 9) is evaluated. This flux divided by 2π as a function of the sphere's radius is plotted in Fig. 12.

The integral is observed to be quantized to integer multiples of 2π. When increasing the radius of the sphere the surface crosses various diabolical points. Each time this happens the flux jumps by $\pm 2\pi$ depending on whether the charge of the Berry curvature monopole is positive or negative. According to Eq. (65), this confirms that the charges of the monopoles created by the point-like degeneracies are $g = \pm 1/2$. Altogether there are six jumps, which means there are six diabolical points in the vicinity of the point P (see Fig. 9). Two of the monopoles in the upper band have a negative, the other four a positive charge of $1/2$. A generic point as the center of the integration sphere is chosen to avoid crossing more than one diabolical point at the time. The deviations from a perfect step function are due to the discretization of the integral, which increases the error when the surface crosses a monopole. The step functions also verify the statement that monopoles are the only possible sources of the Berry curvature.

F. D. M. Haldane [13] describes the dynamics of these degeneracies with respect to the variation of some control parameter, including the creation of a pair of diabolical points and their re-

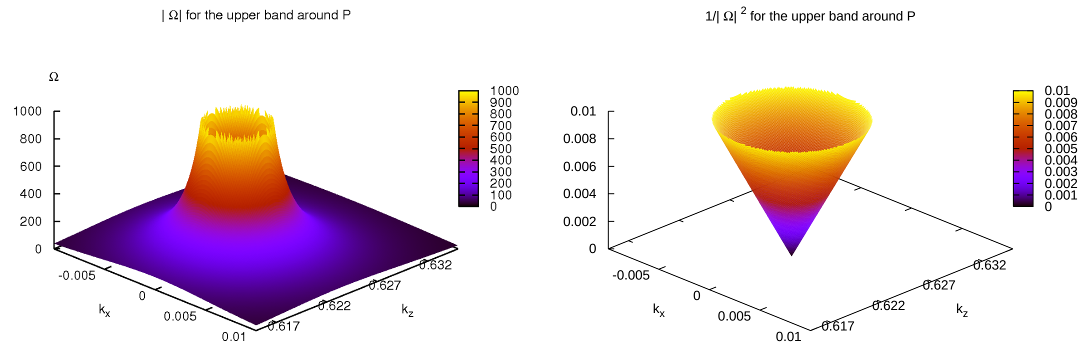

Figure 10: Left: Absolute value of the Berry curvature $|\boldsymbol{\Omega}|$ plotted over a plane in $\mathbf{k}$ space. Right: Inverse square root of the absolut value, i.e., $1/\sqrt{|\boldsymbol{\Omega}|}$.

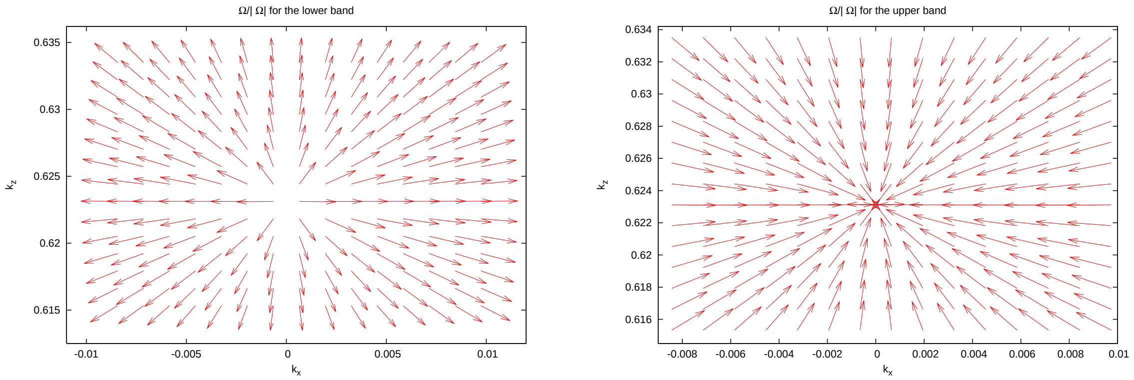

Figure 11: Normalized Berry curvature vector around P (see Fig. 9).

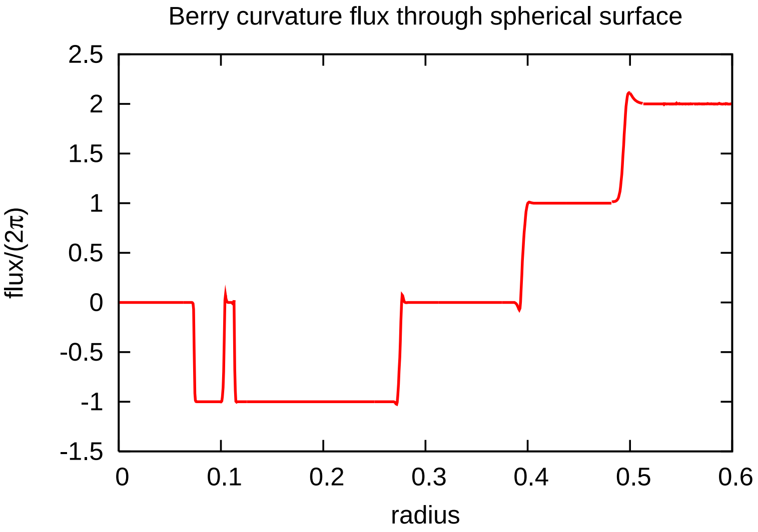

Figure 12: The value of the integral Eq. (65) over a spherical surface for the upper band is plotted against the radius of the sphere.

combination after relative displacement of a reciprocal lattice vector. In the considered case an obvious choice for the control parameters would be λ or V_{xc}, regulating the strength of spin-orbit coupling or exchange splitting, respectively.

Thus, the tight-binding code provides an excellent tool for an investigation of the effects connected with the accidental degeneracy of bands (see for instance, Ref. [13]) since one may scan through a whole range of parameters without consuming much computational resources and still obtain qualitatively reliable results.

2.3 Wannier Interpolation scheme

The first method developed specifically for calculating the Berry curvature of Bloch electrons using the full machinery of the Density Functional Theory (DFT) was based on the Wannier interpolation code of Marzari, Souza and Vanderbilt [25]. As in the case of the KKR method presented in Section 2.1 the essence of this approach by Wang et al. [19] is that it avoids taking the derivative of the periodic part of the Bloch function $u_n(\mathbf{r}, \mathbf{k})$ with respect to $\mathbf{k}$ numerically by finite differences. A second almost equally important feature is that it offers various opportunities to interpolate between different **k** points in the Brillouin zone and hence reducing the number of points at which full *ab initio* calculations need to be performed.

Note that the formulas, naturally arising in wave packet dynamics, for the Berry connection and curvature, given by Eqs. (20) and (21), involve the real space integrals over a unit cell only. Extending them to cover all space by using the Wannier functions defined as

$$|\mathbf{R},\mathbf{n}\rangle = \frac{V_{u.c.}}{(2\pi)^3}\int\limits_{BZ} \mathrm{d}^3\mathrm{k}\; e^{-i\mathbf{k}\cdot\mathbf{R}}\,|\Psi_{\mathbf{k},\mathbf{n}}\rangle\ ,$$

the Bloch theorem and some care with the algebra one finds the following remarkably simple results [19, 26]

$$\mathbf{A}_n(\mathbf{k}) = \sum_{\mathbf{R}} \langle 0n|\,\mathbf{r}\,|\mathbf{R},\mathbf{n}\rangle\, e^{i\mathbf{k}\cdot\mathbf{R}} \quad \text{and} \quad \mathbf{\Omega}_n(\mathbf{k}) = i\sum_{\mathbf{R}} \langle 0n|\,\mathbf{R}\times\mathbf{r}\,|\mathbf{R},\mathbf{n}\rangle\, e^{i\mathbf{k}\cdot\mathbf{R}}\ , \tag{66}$$

where the matrix elements with respect to the Wannier states, as usual, involve integrals over all space. These formulas turn up and play a central role in the method of Wang et al. [19] and make the Wannier interpolation approach looking different from that based on the KKR method which makes use of expansions and integration within a single unit cell only. The lattice sums in Eq. (66) do not have convenient convergence properties, as they depend on the tails of the Wannier functions in real space. By the time an efficient procedure giving "maximally localized" Wannier functions [25, 27] is developed to deal with this issue, where also matrix elements of both $\boldsymbol{\nabla}_{\mathbf{k}}$ and **r**, as in the KKR method discussed in Section (2.1), occur. In fact, reassuringly, it is found in both approaches that an easy to evaluate matrix element of $\boldsymbol{\nabla}_{\mathbf{k}}$ dominates over what is frequently called the dipole contribution involving matrix elements of **r**. The Wannier orbitals are localized, but unlike the orbitals in the tight-binding method, exact representations of the band structure of a periodic solid within this method is possible only for a limited energy range. For metals, its use in modern first-principle calculations is based on the unique "maximally localized orbitals" and its power and achievements are well summarized in a previous Psi-k Highlight [25]. Here we wish to recall only the bare outline of the new development occasioned by the current interest in the geometrical and topological features of the electronic structure of crystals.

The method of Wang et al., well described in Ref. [19], starts with a conventional DFT calculation of Bloch states $|\Psi_{\mathbf{q},n}\rangle$ in a certain energy range and on a selected mesh of **q** points based on plane wave expansion. Then the matrix elements of various operators may be constructed with respect to a set of maximally localized Wannier states $|\mathbf{R},n\rangle$. Noting that the phase sum

$$|u_n^W(\mathbf{k})\rangle = \sum_{\mathbf{R}} e^{-i\mathbf{k}\cdot(\mathbf{r}-\mathbf{R})}\,|\mathbf{R},n\rangle \tag{67}$$

of these states can be defined for an arbitrary **k** point, which may be at or in between the first principles **q**-point mesh, and regarded as a "Wannier gauge" representation of the periodic part of a Bloch state, one has to construct the following matrix elements

$$\begin{aligned}
H^W_{nm}(\mathbf{k}) &= \sum_{\mathbf{R}} e^{+i\mathbf{k}\cdot\mathbf{R}} \langle \mathbf{0},n| \widehat{H} |\mathbf{R},m\rangle \ , \\
\boldsymbol{\nabla} H^W_{nm}(\mathbf{k}) &= \sum_{\mathbf{R}} e^{+i\mathbf{k}\cdot\mathbf{R}} i\mathbf{R} \langle \mathbf{0},n| \widehat{H} |\mathbf{R},m\rangle \ , \\
\mathbf{A}^W_{nm}(\mathbf{k}) &= \sum_{\mathbf{R}} e^{+i\mathbf{k}\cdot\mathbf{R}} \langle \mathbf{0},n| \mathbf{r} |\mathbf{R},m\rangle \ , \\
\boldsymbol{\Omega}^W_{nm}(\mathbf{k}) &= i\sum_{\mathbf{R}} e^{+i\mathbf{k}\cdot\mathbf{R}} \langle \mathbf{0},n| \mathbf{R}\times\mathbf{r} |\mathbf{R},m\rangle \ .
\end{aligned} \tag{68}$$

Actually, all of them are given in the same "Wannier gauge". The indices n and m refer to the full bundle, mainly the occupied, bands selected for the representation.
The next step is to find a unitary matrix $\bar{\bar{U}}(\mathbf{k})$ such that

$$\bar{\bar{U}}^\dagger(\mathbf{k})\bar{\bar{H}}^W(\mathbf{k})\ \bar{\bar{U}}(\mathbf{k}) = \bar{\bar{H}}^H(\mathbf{k}) \ \ \text{with} \ \ H^H_{nm}(\mathbf{k}) = \mathcal{E}_{n\mathbf{k}}\delta_{nm} \ , \tag{69}$$

where the eigenvalue $\mathcal{E}_{n\mathbf{k}}$ should agree with the first-principles dispersion relation of the bands chosen to be represented. The corresponding eigenfunctions

$$\left|u^H_n(\mathbf{k})\right\rangle = \sum_m U_{nm}(\mathbf{k}) \left|u^W_m(\mathbf{k})\right\rangle \tag{70}$$

should reproduce the periodic part of these states.
Thus, $|u^H_n(\mathbf{k})\rangle$ can be used to evaluate Eqs. (20) and (21) for the Berry connection and the curvature in the standard way. However, such direct calculations are precisely not what one would like to do. The point of Wang et al. is that the above preamble offers an alternative. Namely, the unitary transformation $\bar{\bar{U}}(\mathbf{k})$ transforms all states and operators from the "Wannier gauge" to another gauge which is called "Hamiltonian (H) gauge" and one can transform all the easy to evaluate "Wannier gauge" operators in Eq. (68) into their "Hamiltonian gauge" form. Of course, $\boldsymbol{\Omega}^H_{nm}(\mathbf{k})$ is of particular interest. Unfortunately, due to the $\mathbf{k}$ dependence of $U_{nm}(\mathbf{k})$ the form of Eqs. (20) and (21) is not covariant under such transformation. For instance

$$\mathbf{A}^H = U^\dagger \mathbf{A}^W U + U^\dagger \boldsymbol{\nabla} U = \overline{\mathbf{A}}^H + U^\dagger \boldsymbol{\nabla} U, \tag{71}$$

where for clarity the momentum and band index dependences have been suppressed. A similar, but more complicated formula can be derived for $\boldsymbol{\Omega}^H$. Denoting $\overline{\mathbf{A}}^H$, and $\overline{H}^H$ the covariant components, that is to say the part of the transformed operator which does not contain $U^\dagger\boldsymbol{\nabla}U$, of $\mathbf{A}^H$ and H^H, respectively and

$$\mathbf{D}^H_{nm} = \left(U^\dagger \boldsymbol{\nabla} U\right)_{nm} = \frac{\boldsymbol{\nabla}\overline{H}^H_{nm}}{\mathcal{E}_m - \mathcal{E}_n}(1-\delta_{nm}) \ , \tag{72}$$

the final formula for the Berry curvature reads as follows ($\overline{\boldsymbol{\Omega}}^H = U^\dagger \boldsymbol{\Omega}^W U$)

$$\boldsymbol{\Omega}(\mathbf{k}) = \sum_n f_n \overline{\boldsymbol{\Omega}}^H_{nn}(\mathbf{k}) + \sum_{n,m} (f_m - f_n)\, \mathbf{D}^H_{nm} \times \overline{\mathbf{A}}^H_{mn} + \boldsymbol{\Omega}^{DD}(\mathbf{k}) \ , \tag{73}$$

where the last term takes the following form

$$\boldsymbol{\Omega}^{DD}(\mathbf{k}) = i\sum_{nm} (f_m - f_n) \frac{\boldsymbol{\nabla}\overline{H}^H_{nm}(\mathbf{k}) \times \boldsymbol{\nabla}\overline{H}^H_{mn}(\mathbf{k})}{\left(\mathcal{E}_m - \mathcal{E}_n\right)^2} \ . \tag{74}$$

Here f_n and f_m are the distribution functions for band n and m, respectively. Interestingly, this is the standard form of the Berry curvature for a Hamiltonian which depends parametrically on $\mathbf{k}$ and it also shows up as one of the contributions in the KKR and the tight-binding approaches discussed in Sections. 2.1 and 2.2 . Reassuringly, computations by all three methods find the contribution from such terms to the total curvature dominant and almost exclusively responsible for the surprisingly spiky features as functions of $\mathbf{k}$. As noted in the introduction, these features originate from band crossings or avoided crossings and have a variety of interesting physical consequences.

For instance, the Berry curvature calculated by Wang et al. [19, 28], shown in Fig. 13, leads directly to a good quantitative account of the intrinsic contribution to the anomalous Hall effect in Fe. The left panel of Fig. 13 shows the decomposition of the Berry curvature in different contributions arising from the expansion of the states into a Wannier basis (see Eq. (73)). Noting the logarithmic scale, it is evident that the dominant contribution stems from the Berry curvature $\mathbf{\Omega}^{DD}(\mathbf{k})$ of the $\mathbf{k}$-dependent Hamiltonian $\overline{H}^H(\mathbf{k})$ according to Eq. (74). The other terms including matrix elements of the position operator $\mathbf{r}$ are negligible, which is similar to what turned out to be the case within the KKR method. Further, applications of the considered method to the cases of fcc Ni and hcp Co [28, 29] are equally impressive.

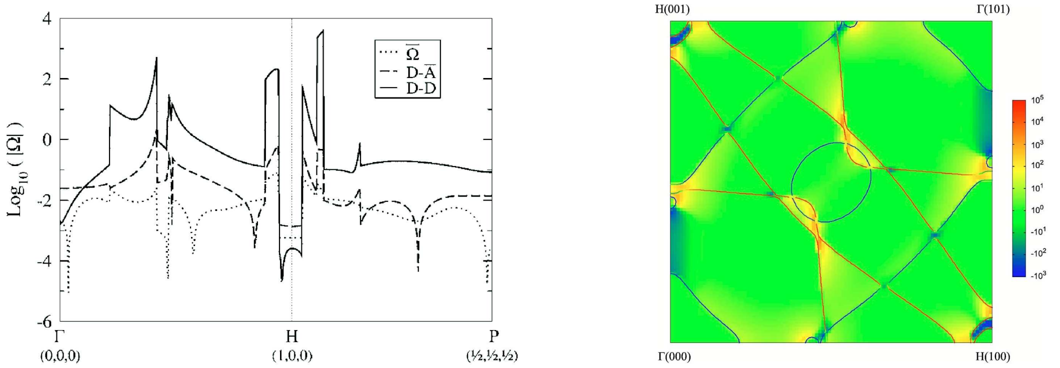

Figure 13: Left: Berry curvature $\Omega^z(\mathbf{k})$ of Fe along symmetry lines with a decomposition in three different contributions of Eq. (73) (note the logarithmic scale). Right: Fermi surface in (010) plane (solid lines) and Berry curvature $-\Omega^z(\mathbf{k})$ in atomic units (color map) [19].

2.4 Kubo formula

2.4.1 Anomalous Hall conductivity or charge Berry curvature

Most conventional approaches to the electronic transport in solids are based on the very general linear response theory of Kubo [30]. Indeed, the first insight into the cause of the anomalous Hall effect by Karplus and Luttinger [31] was gained by deploying the Kubo formula for a simple model Hamiltonian of electrons with spin. In this Section we review briefly the first principles implementation of the Kubo formula in aid of calculating the Berry curvature. The simple observation which makes this possible is that both the semiclassical description and the Kubo formula approach yield an expression for the intrinsic contribution to the anomalous Hall conductivity (AHC). Hence by comparing the two a Kubo-like expression for the Berry curvature can be extracted. Here we examine the formal connection between the two formulas and demonstrate that they are equivalent as was mentioned already by Wang et al. [19]. The starting point is the Berry curvature written in terms of the periodic part of the Bloch function

$$\mathbf{\Omega}_n(\mathbf{k}) = i \left\langle \boldsymbol{\nabla} u_n(\mathbf{k}) \right| \times \left| \boldsymbol{\nabla} u_n(\mathbf{k}) \right\rangle \ . \tag{75}$$

Let us follow the route given by M. V. Berry [2] to rewrite this expression. Introducing the completeness relation with respect to the N present bands, $1 = \sum_{n'} |u_{n'}\rangle \langle u_{n'}|$, excluding the vanishing term with $n' = n$ and using the relation

$$\langle \boldsymbol{\nabla} u_n(\mathbf{k}) | u_{n'}(\mathbf{k}) \rangle = \frac{\langle u_n(\mathbf{k}) | \, \boldsymbol{\nabla} H(\mathbf{k}) \, | u_{n'}(\mathbf{k}) \rangle}{\mathcal{E}_n(\mathbf{k}) - \mathcal{E}_{n'}(\mathbf{k})} \ , \tag{76}$$

which follows from $\langle u_n(\mathbf{k}) | \, H(\mathbf{k}) \, | u_{n'}(\mathbf{k}) \rangle = \mathcal{E}_{n'}(\mathbf{k}) \langle u_n(\mathbf{k}) | u_{n'}(\mathbf{k}) \rangle = 0$, yields

$$\mathbf{\Omega}_n(\mathbf{k}) = i \sum_{n' \neq n} \frac{\langle u_n(\mathbf{k}) | \, \boldsymbol{\nabla} H(\mathbf{k}) \, | u_{n'}(\mathbf{k}) \rangle \times \langle u_{n'}(\mathbf{k}) | \, \boldsymbol{\nabla} H(\mathbf{k}) \, | u_n(\mathbf{k}) \rangle}{\left(\mathcal{E}_n(\mathbf{k}) - \mathcal{E}_{n'}(\mathbf{k}) \right)^2} \ . \tag{77}$$

If we reformulate it with respect to the Bloch functions

$$\mathbf{\Omega}_n(\mathbf{k}) = i \sum_{n' \neq n} \frac{\langle \Psi_{n\mathbf{k}} | e^{i\mathbf{kr}} \boldsymbol{\nabla} H(\mathbf{k}) e^{-i\mathbf{kr}} | \Psi_{n'\mathbf{k}} \rangle \times \langle \Psi_{n'\mathbf{k}} | e^{i\mathbf{kr}} \boldsymbol{\nabla} H(\mathbf{k}) e^{-i\mathbf{kr}} | \Psi_{n\mathbf{k}} \rangle}{\left(\mathcal{E}_n(\mathbf{k}) - \mathcal{E}_{n'}(\mathbf{k}) \right)^2} \tag{78}$$

and use the relations

$$H(\mathbf{k}) = e^{-i\mathbf{kr}} \hat{H} e^{i\mathbf{kr}} \ , \tag{79}$$

$$\boldsymbol{\nabla} H(\mathbf{k}) = i e^{-i\mathbf{kr}} \left[\hat{H} \mathbf{r} - \mathbf{r} \hat{H} \right] e^{i\mathbf{kr}} = \hbar \ e^{-i\mathbf{kr}} \hat{\mathbf{v}} e^{i\mathbf{kr}} \ , \tag{80}$$

we end up with a Kubo-like formula widely used in the literature [40, 41]

$$\mathbf{\Omega}_n(\mathbf{k}) = i\hbar^2 \sum_{n' \neq n} \frac{\langle \Psi_{n\mathbf{k}} | \hat{\mathbf{v}} | \Psi_{n'\mathbf{k}} \rangle \times \langle \Psi_{n'\mathbf{k}} | \hat{\mathbf{v}} | \Psi_{n\mathbf{k}} \rangle}{\left(\mathcal{E}_n(\mathbf{k}) - \mathcal{E}_{n'}(\mathbf{k}) \right)^2} \ . \tag{81}$$

Here all occupied and unoccupied states have to be accounted in the sum. An important feature of this form is that it is expressed in terms of the off-diagonal matrix elements of the velocity operator with respect to the Bloch states. To deal with them a technique was adopted, which served well for computing the optical conductivities [32, 33], where the same matrix elements have been required.

The first *ab initio* calculation of the Berry curvature was actually performed for $\mathrm{SrRuO_3}$ by Fang et al. [34] using Eq. (81) . The authors nicely illustrate the existence of a magnetic monopole in the crystal momentum space, which is shown in Fig. 14. The origin of this sharp structure is the near degeneracy of bands. It acts as a magnetic monopole. A similar effect was found for Fe by Yao et al. [35]. They demonstrate that for **k** points near the spin-orbit driven avoided crossings of the bands the Berry curvature is extremely enhanced, shown in Fig. 15. In addition, the agreement between the right panels of Fig. 13 and Fig. 15 shows impressively the equivalence between the two different methods.

2.4.2 Spin Hall conductivity or the so-called spin Berry curvature

Of course, the fact that the results of the semiclassical transport theory and the quantum mechanical Kubo formula agree exactly, as was shown above for the AHC, is surprising. In

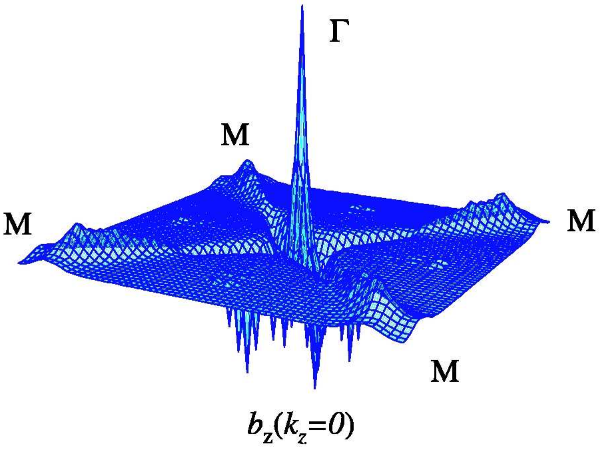

Figure 14: Calculated flux b_z (corresponds to Berry curvature Ω^z) distribution in $\mathbf{k}$ space for t_{2g} bands as a function of (k_x, k_y) with $k_z = 0$ for SrRuO$_3$ with cubic structure [34].

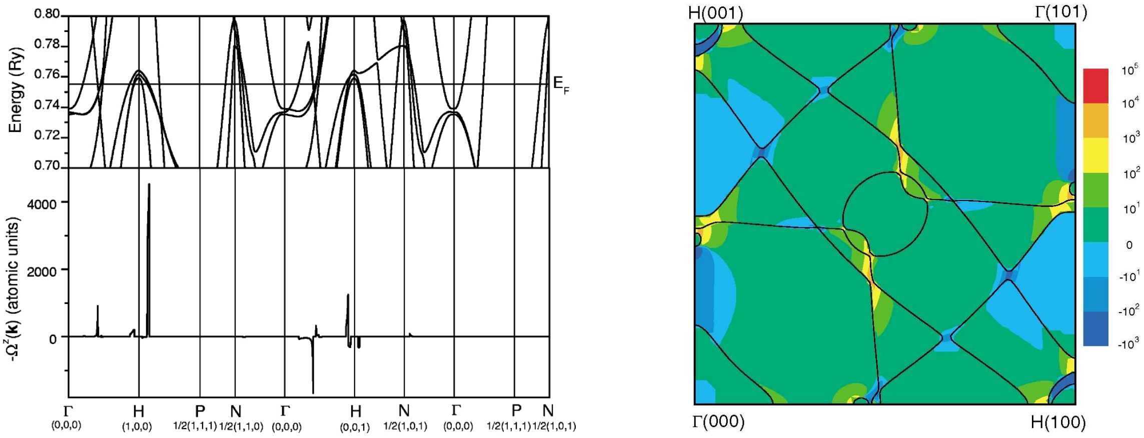

Figure 15: Left: Band structure of bulk Fe near Fermi energy (upper panel) and Berry curvature $\Omega^z(\mathbf{k})$ (lower panel) along symmetry lines. Right: Fermi surface in (010) plane (solid lines) and Berry curvature $-\Omega^z(\mathbf{k})$ in atomic units (color map) [35].

general, it cannot be expected for all transport coefficients. Indeed, as we shall now demonstrate, the situation is quite different for the spin Hall conductivity.

Evidently, the Kubo approach is readily adopted to calculate the spin current response to an external electric field $\mathbf{E}$. Although there is still a controversy about an expression for the spin-current operator to be taken [36–39], frequently the symmetrized tensor product of the spin operator $\hat{\boldsymbol{\Sigma}}$ and the velocity operator $\hat{\mathbf{v}}$ is used. Namely, the spin current response is calculated as the expectation value of the operator

$$\hat{\mathbf{J}}^{\mathrm{Spin}} = \frac{1}{2}\left(\hat{\beta}\hat{\boldsymbol{\Sigma}} \otimes \hat{\mathbf{v}} + \hat{\mathbf{v}} \otimes \hat{\beta}\hat{\boldsymbol{\Sigma}}\right) \tag{82}$$

Using the same argument as for the calculation of the charge Hall conductivity, one finds [37, 40, 41]

$$\sigma^z_{xy} = \frac{e^2}{\hbar}\sum_{\mathbf{k},\mathbf{n}} \sigma^z_{yx;n}(\mathbf{k}) \ , \tag{83}$$

where the $\mathbf{k}$ and band resolved conductivity $\sigma^z_{yx;n}(\mathbf{k})$ in the framework of the Kubo formula (Ku) is given by

$$\sigma^z_{yx;n}(\mathbf{k})_{\mathrm{Ku}} = i\hbar^2 \sum_{n'\neq n} \frac{\langle \Psi_{n\mathbf{k}}| \hat{\beta}\hat{\Sigma}_z \hat{v}_y |\Psi_{n'\mathbf{k}}\rangle \times \langle \Psi_{n'\mathbf{k}}| \hat{v}_x |\Psi_{n\mathbf{k}}\rangle}{(\mathcal{E}_n(\mathbf{k}) - \mathcal{E}_{n'}(\mathbf{k}))^2} \ . \tag{84}$$

In the literature, this quantity is sometimes even called spin Berry curvature [41] analogously to the AHE. As will be shown now, this notation is misleading and should not be used.
Of course, one may tackle the same problem from the point of view of the semiclassical theory (sc). This suggests that one should take the velocity in Eq. (82) to be the anomalous velocity given by Eq. (11). This argument leads to [4, 36]

$$\sigma^z_{yx;n}(\mathbf{k})_{\mathrm{sc}} = \mathrm{Tr}\left[\bar{\bar{S}}^n(\mathbf{k})\bar{\bar{\Omega}}^z_n(\mathbf{k})\right] \ . \tag{85}$$

Here $S^n_{ij}(\mathbf{k}) = \langle i, \mathbf{k}|\hat{\beta}\hat{\Sigma}_z|j, \mathbf{k}\rangle$ is the spin matrix for a Kramers pair and $\bar{\bar{\Omega}}^z_n(\mathbf{k})$ is the non-Abelian Berry curvature [20] introduced in Section 1.3. The point we wish to make here is that this formula is not equivalent to the Kubo form in Eq. (84) because band off-diagonal terms of the spin matrix were neglected in the derivation from the wave packet dynamics of Eq. (85) [4].
Evidently, $\sigma^z_{yx;n}(\mathbf{k})_{\mathrm{Ku}}$ can not be written as a single band expression, in contrast to the case of the AHC which turned out to be exactly the conventional Berry curvature (see Section 2.4.1). The contributions of Eq. (84) which were neglected in Eq. (85) are of quantum-mechanical origin and are not accounted for in the semiclassical derivation. Culcer et al. [36] tackled the problem and identified the neglected contributions, without giving up the wave packet idea, as spin and torque dipole terms. Nevertheless, it was shown [20] that under certain approximations a semiclassical description may result in quantitatively comparable results to the Kubo approach. This will be discussed in the next section.

3 Intrinsic contribution to the charge and spin conductivity in metals

Here we discuss applications of the computational methods for the Berry curvature discussed in the previous Section. We will focus on first principles calculations of the anomalous and spin Hall conductivity.
The first *ab initio* studies of the AHE, based on the Kubo formula

$$\sigma_{xy} = -\frac{e^2}{\hbar}\sum_n \int_{BZ} \frac{\mathrm{d}^3\mathrm{k}}{(2\pi)^3} f_n(E_F, \mathbf{k})\Omega^z_n(\mathbf{k}) \tag{86}$$

with $\mathbf{\Omega}_n(\mathbf{k})$ defined by Eq. (81), were reported in Refs. [34, 42]. As it is well known, the conventional expression for the Hall resistivity

$$\rho_{xy} = R_0 B + 4\pi R_s M \tag{87}$$

(where B is the magnetic field, R_0 and R_s are the normal and the anomalous Hall coefficient, respectively) assumes a monotonic behavior of ρ_{xy} as well as σ_{xy} as a function of the magnetization M. By means of first principles calculations based on the pseudopotential method (STATE code), Z. Fang et al. [34] have shown that the unconventional nonmonotonic behavior of the AHC measured in $SrRuO_3$ (Fig. 16, left) is induced by the presence of a *magnetic monopole* (MM) in momentum space (see Fig. 14 and the corresponding discussion). The existence of MMs causes the sharp and spiky structure of the AHC as a function of the Fermi-level position, shown in the right panel of Fig. 16. At the self-consistently determined Fermi level the calculated value $\sigma_{xy} = -60\ (\Omega cm)^{-1}$ is comparable with the experimentally observed conductivity of about $-100\ (\Omega cm)^{-1}$. Obviously, a small change in the Fermi level would cause dramatic changes in the resulting AHC. Indeed, as it was shown in Ref. [42], the AHC of ferromagnetic $Gd_2Mo_2O_7$ and $Nd_2Mo_2O_7$ is strongly changed by the choice of the Coulomb repulsion U varied in the used mean-field Hartree-Fock approach.

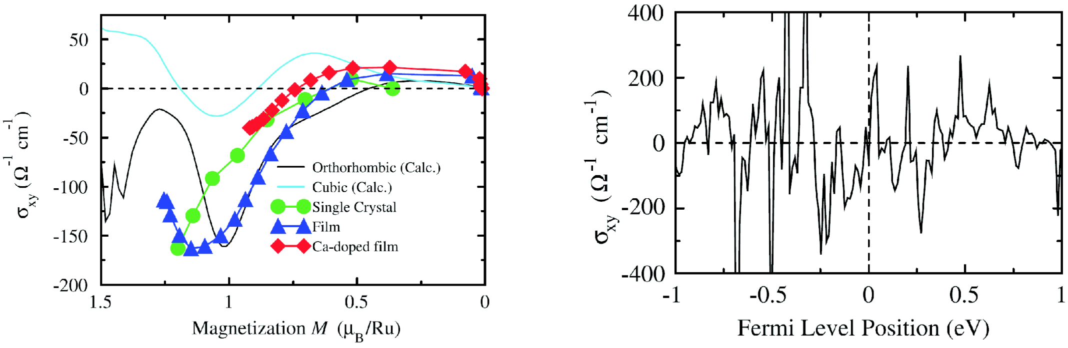

Figure 16: Left: The Hall conductivity σ_{xy} of $SrRuO_3$ as a function of the magnetization; Right: σ_{xy} as a function of the Fermi-level position for the orthorhombic structure of $SrRuO_3$. [34].

A year later, results for the AHC in ferromagnetic bcc Fe, based on the full-potential linearized augmented plane-wave method (WIEN2K code) were published [35]. The authors used the same Kubo formula approach to describe the transversal transport. In particular, a close agreement between theory, $\sigma_{xy} = 751\ (\Omega cm)^{-1}$, and experiment, $\sigma_{xy} = 1032\ (\Omega cm)^{-1}$, was found that points to the dominance of the intrinsic contribution in Fe. A slow convergence of the calculated value for the AHC with respect to the number of $\mathbf{k}$ points was reported. The reason for the convergence problems are small regions in momentum space around avoided crossings and enhanced spin-orbit coupling. In the behavior of the Berry curvature these points cause strong peaks which is shown in Fig. 15. If both related states of the avoided crossing are occupied their combined contribution to the AHC is negligible since they compensate each other. However, when the Fermi level lies in a spin-orbit induced gap then the occupied state, which acts now as an isolated magnetic monopole, causes a peak in the AHC. Consequently, it was necessary to use millions of $\mathbf{k}$ points in the first Brillouin zone to reach convergence.

To avoid such demanding computational efforts, the Wannier interpolation scheme, discussed in Section 2.3, was suggested and applied for Fe in Ref. [19]. The authors started with the relativistic electronic structure obtained by the pseudopotential method (PWSCF code) at a relatively coarse $\mathbf{k}$ mesh. Using maximally localized Wannier functions, constructed from the obtained Bloch states, all quantities of interest were expressed in the tight-binding like basis and interpolated onto a dense $\mathbf{k}$ mesh. Then this new mesh was used to calculate the AHC. The obtained value of $756\ (\Omega cm)^{-1}$ is in good agreement with the result of Ref. [35], (see above).

The same scheme was used further on to calculate the AHC applying Haldane's formula [13] which means integration not over the entire Fermi sea, as it is required by the Kubo formula, but only over the Fermi surface. The results obtained for Fe, Co, and Ni [28] agreed very well for both procedures and with previous theoretical studies [35]. Moreover, the work done by the group of D. Vanderbilt [19] has stimulated further first-principles calculations as will be shown below.

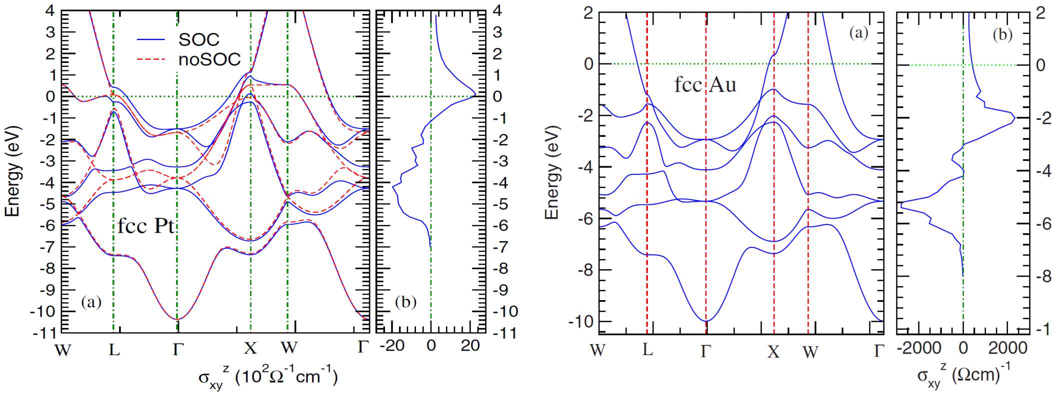

Figure 17: Left: (a) Relativistic band structure and (b) spin Hall conductivity of fcc Pt [43]; Right: (a) Relativistic band structure and (b) spin Hall conductivity of fcc Au [44]. The dashed curves in the left panel represent the scalar-relativistic band structure.

The first *ab initio* calculations of the spin Hall conductivity (SHC) were performed for semiconductors and metals [40, 41]. The description of the electronic structure in Ref. [41] was based on the full-potential linearized augmented plane-wave method (WIEN2K code) and in Ref. [40] on the all-electron linear muffin-tin orbital method, but both rely on the solution of the Kubo formula given by Eq. (84) to describe the SHC. Later, in Ref. [43] the relatively large SHC measured in Pt was explained by the contribution of the spin-orbit split d bands at the high-symmetry points L and X near the Fermi level (Fig. 17, left). In contrast, Au [44] shows similar contributions to the SHC, but at too low energies with respect to E_F. Since the extra electron of Au with respect to Pt causes full occupation of the d bands (Fig. 17, right).

The spin-orbit coupling is the origin of the AHE and SHE. In particular, the avoided crossings significantly increase the effect. In addition, the spin-orbit coupling links the spin degree of freedom to the crystal lattice, which is the source of the anisotropy with respect to the chosen quantization axis. This was demonstrated first for the AHE in hcp Co [29] and later for the SHE in several nonmagnetic hcp metals [45] (Fig. 18). Here, the pseudopotential method (PWSCF code) and the full-potential linearized augmented-plane-wave method (FLEUR code) were used for the AHE and SHE, respectively. To reduce the computational efforts, the Berry curvature calculations were based on the Wannier interpolation scheme according to Ref. [19].

Finally, an approach for calculating the SHC based on the KKR method was proposed (Ref. [20], Section 2.1). For the description of the transversal spin transport the authors applied an approach different from the widely used Kubo formula. Their calculations are based on the expression for the SHC in the non-Abelian case suggested in Ref. [4]. This expression was simplified further by the approximation that the expectation value of the $\beta\Sigma_z$ operator is assumed to be

+1 and −1 for the two spin degenerate states, arising in nonmagnetic crystals with inversion symmetry. Thus, the semiclassical treatment was reduced to the two current model with the final expression for the SHC in terms of the usual formula for the AHC

$$\sigma_{xy}^{z} = \frac{e^2}{\hbar(2\pi)^3} \int^{E_F} d\mathcal{E}\ \Omega^z(\mathcal{E}) \ , \tag{88}$$

where $\Omega^z\,(\mathcal{E})$ is defined by Eq. (55). The spin Hall conductivities $\sigma_{xy}^{z}(\mathcal{E})$, calculated for Pt and Au in such an approach (Fig. 19), are quantitatively in good agreement to the ones obtained by the Kubo-like formula (see Fig. 17).

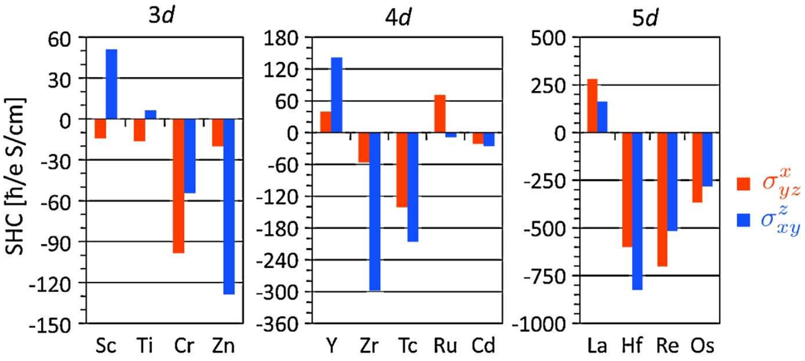

Figure 18: Spin Hall conductivities σ_{yz}^{x} and σ_{xy}^{z} for several hcp metals and for antiferromagnetic Cr [45].

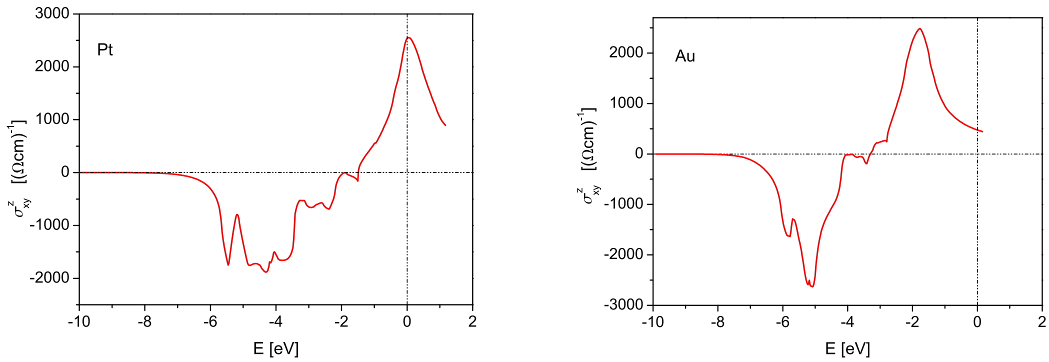

Figure 19: The spin Hall conductivity for fcc Pt (left) and Au (right) [20].

4 Conclusion

In the presence of a periodic crystal potential the free electron spectrum $\mathcal{E}_{\mathbf{k}} = \frac{\hbar^2 k^2}{2m}$ breaks up into bands with complex dispersion relation $\mathcal{E}_{n\mathbf{k}}$. It turns out that consistent adiabatic dynamics of wave packets constructed by superposition of states for all $\mathbf{k}$ but a limited number of bands features a Berry connection $\mathbf{A}_n(\mathbf{k})$ and a corresponding curvature $\mathbf{\Omega}_n(\mathbf{k})$ which account for the influence of the neglected bands [5, 16]. Moreover, these geometrical properties of the band structure play an essential role in describing a number of important physical phenomena such as spin and charge transport, electric polarization and orbital magnetization [1]. What makes these remarkable developments particularly interesting from the point of view of *first-principles* electronic structure calculations is the fact that the curvature $\mathbf{\Omega}_n(\mathbf{k})$ is a very rapidly varying function of $\mathbf{k}$ and it depends on intricate details of the band structure. Consequently, devising methods for computing $\mathbf{\Omega}_n(\mathbf{k})$ have recently become a very active field of research. In this paper we sketched three approaches to the problem: one is based on Multiple Scattering Theory (KKR, LMTO), another one on the Wannier function representation of *first-principles* bands and the third one on direct evaluation of a Kubo like formula. We pointed out the differences and highlighted the similarities in the way the derivatives with respect to the wave vector $\mathbf{k}$ enter the problem. We stressed the importance of level crossings which give rise to curvatures $\mathbf{\Omega}_n(\mathbf{k})$ whose $\mathbf{k}$ dependence is that of the Dirac monopole and the more exotic avoided crossings of Kramers degenerate bands whose curvature is a non-Abelian gauge field. As illustrations of results by the various methods, we presented calculations of the intrinsic contribution to the anomalous and spin Hall conductivity as well as the Berry curvature for a variety of systems.

Hopefully, it has been demonstrated that more work is needed to make quantitative contact with experiments on more complex materials and transport phenomena other then those we had occasion to mention. From the computational point of view the spatial and temporal like curvatures, will represent new challenges.

References

[1] D. Xiao, M.-C. Chang, and Q. Niu, *Berry phase effects on electronic properties*, Rev. Mod. Phys. **82**, 1959 (2010).

[2] M. V. Berry, *Quantal phase factors accompanying adiabatic changes*, Proc. Roy. Soc. A (London) **392**, 45 (1984).

[3] D. Culcer, Y. Yao and Q. Niu, *Coherent wave-packet evolution in coupled bands*, Phys. Rev. B **72**, 085110 (2005).

[4] R. Shindou and K.-I. Imura, *Noncommutative geometry and non-Abelian Berry phase in the wave-packet dynamics of Bloch electrons*, Nuclear Phys. B **720**, 399-435 (2005).

[5] F. Wilczek and A. Zee, *Appearance of Gauge Structure in Simple Dynamical Systems*, Phys. Rev. Lett. **52**, 2111 (1984).

[6] H. A. Kramers, *General Theory of Paramagnetic Rotation in Crystals*, Proc. R. Acad. Sci. Amsterdam **33**, 959 (1930).

[7] R. J. Elliott, *Theory of the Effect of Spin-Orbit Coupling on Magnetic Resonance in Some Semiconductors*, Phys. Rev. **96**, 266 (1954).

[8] M. V. Berry and M. Wilkinson, *Diabolical Points in the Spectra of Triangles*, Proc. Roy. Soc. (Londond) **392**, 15 (1984).

[9] P. A. M. Dirac, *The Theory of Magnetic Poles*, Phys. Rev., **74**, 817 (1948).

[10] K. M. D. Hals, A. K. Nguyen, X. Waintal, and A. Brataas, *Effective Magnetic Monopoles and Universal Conductance Fluctuations*, Phys. Rev. Lett. **105**, 207204 (2010).

[11] D. J. Thouless, M. Kohmoto, M. P. Nightingale, and M. den Nijs, *Quantized Hall Conductance in a Two-Dimensional Periodic Potential*, Phys. Rev. Lett. **49**, 405 (1982).

[12] B. Simon, *Holonomy, the Quantum Adiabatic Theorem, and Berry's Phase*, Phys. Rev. Lett. **51**, 2167 (1983).

[13] F. D. M. Haldane, *Berry Curvature on the Fermi Surface: Anomalous Hall Effect as a Topological Fermi-Liquid Property*, Phys. Rev. Lett. **93**, 206602 (2004).

[14] J. von Neumann and E. Wigner, *Über das Verhalten von Eigenwerten bei adiabatischen Prozessen*, Phys. Z. **30**, 467 (1929).

[15] A. Bohm, A. Mostafazadeh, H. Koizumi, Q. Niu, and J. Zwanziger, *The Geometric Phase in Quantum Systems*, Springer-Verlag, Berlin (2003).

[16] G. Sundaram and Q. Niu, *Wave-packet dynamics in slowly perturbed crystals: Gradient corrections and Berry-phase effects*, Phys. Rev. B **59**, 14915 (1999).

[17] M. Gradhand, M. Czerner, D.V. Fedorov, P. Zahn, B. Yu. Yavorsky, L. Szunyogh, and I. Mertig, *Spin polarization on Fermi surfaces of metals by the KKR method*, Phys. Rev. B **80**, 224413 (2009).

[18] J. Fabian and S. Das Sarma, *Spin Relaxation of Conduction Electrons in Polyvalent Metals: Theory and a Realistic Calculation*, Phys. Rev. Lett. **81**, 5624 (1998).

[19] X. Wang, J. R. Yates, I. Souza, and D. Vanderbilt, *Ab initio calculation of the anomalous Hall conductivity by Wannier interpolation*, Phys. Rev. B **74**, 195118 (2006).

[20] M. Gradhand, D.V. Fedorov, F. Pientka, P. Zahn, I. Mertig, and B.L. Györffy, *On calculating the Berry curvature of Bloch electrons using the KKR method*, Phys. Rev. B, *submitted* (2011) .

[21] R. Zeller, P. H. Dederichs, B. Újfalussy, L. Szunyogh, P. Weinberger, *Theory and convergence properties of the screened Korringa-Kohn-Rostoker method*, Phys. Rev. B **52**, 8807 (1995).

[22] P. Strange, *Relativistic Quantum Mechanics with applications in condensed Matter and atomic physics*, (Cambridge University Press, 1998).

[23] J. C. Slater and G. F. Koster, *Simplified LCAO Method for the Periodic Potential Problem*, Phys. Rev. **94**, 1498 (1954).

[24] M. D. Jones and R. C. Albers, *Spin-orbit coupling in an f-electron tight-binding model: Electronic properties of Th, U, and Pu*, Phys. Rev. B **79**, 045107 (2009).

[25] N. Marzari, I. Souza, and D. Vanderbilt, *An Introduction to Maximally-Localized Wannier Functions*, Psi-k Newsletter **57**, Scientific Highlight of the month (2003).

[26] F. Pientka, *Geometrical Concepts in the Band Theory of Solids*, Diploma thesis, University Halle-Wittenberg (2010).

[27] N. Marzari and D. Vanderbilt, *Maximally localized generalized Wannier functions for composite energy bands*, Phys. Rev. B **56**, 12847 (1997).

[28] X. Wang, D. Vanderbilt, J. R. Yates, and I. Souza, *Fermi-surface calculation of the anomalous Hall conductivity*, Phys. Rev. B **76**, 195109 (2007).

[29] E. Roman, Y. Mokrousov, and I. Souza, *Orientation Dependence of the Intrinsic Anomalous Hall Effect in hcp Cobalt*, Phys. Rev. Lett. **103**, 097203 (2009).

[30] R. Kubo, *Statistical-Mechanical Theory of Irreversible Processes*, J. Phys. Soc. Japan **12**, 570 (1957).

[31] R. Karplus and J. M. Luttinger, *Hall Effect in Ferromagnetics*, Phys. Rev. **95**, 1154 (1954).

[32] C. S. Wang and J. Callaway, *Band structure of nickel: Spin-orbit coupling, the Fermi surface, and the optical conductivity*, Phys. Rev. B **9**, 4897 (1974).

[33] G. Y. Guo and H. Ebert, *Band-theoretical investigation of the magneto-optical Kerr effect in Fe and Co multilayers*, Phys. Rev. B **51**, 12633 (1995).

[34] Z. Fang, N. Nagaosa, K. S. Takahashi, A. Asamitsu, R. Mathieu, T. Ogasawara, H. Yamada, M. Kawasaki, Y. Tokura, K. Terakura, *The Anomalous Hall Effect and Magnetic Monopoles in Momentum Space*, Science **302**, 92 (2003).

[35] Y. Yao, L. Kleinman, A.H. MacDonald, J. Sinova, T. Jungwirth, D. Wang, E. Wang, and Q. Niu, *First Principles Calculation of Anomalous Hall Conductivity in Ferromagnetic bcc Fe*, Phys. Rev. Lett. **92**, 037204 (2004).

[36] D. Culcer, J. Sinova, N. A. Sinitsyn, T. Jungwirth, A. H. MacDonald, and Q. Niu, *Semiclassical Spin Transport in Spin-Orbit-Coupled Bands*, Phys. Rev. Lett. **93**, 046602 (2004).

[37] J. Sinova. D. Culcer, Q. Niu, N. A. Sinitsyn, T. Jungwirth, and A. H. MacDonald, *Universal Intrinsic Spin Hall Effect*, Phys. Rev. Lett. **92**, 126603 (2004).

[38] A. Vernes, B. L. Györffy, and P. Weinberger, *Spin currents, spin-transfer torque, and spin-Hall effects in relativistic quantum mechanics*, Phys. Rev. B **76**, 012408 (2007).

[39] S. Lowitzer, M. Gradhand, D. Ködderitzsch, D.V. Fedorov, I. Mertig, H. Ebert, *Extrinsic and Intrinsic Contributions to the Spin Hall Effect of Alloys*, Phys. Rev. Lett. **106**, 056601 (2011).

[40] G. Y. Guo, Y. Yao, and Q. Niu, *Ab initio Calculation of the Intrinsic Spin Hall Effect in Semiconductors*, Phys. Rev. Lett. **94**, 226601 (2005).

[41] Y. Yao and Z. Fang, *Sign Changes of Intrinsic Spin Hall Effect in Semiconductors and Simple Metals: First-Principles Calculations*, Phys. Rev. Lett. **95**, 156601 (2005).

[42] I. V. Solovyev, *Effects of crystal structure and on-site Coulomb interactions on the electronic and magnetic structure of $A_2Mo_2O_7$ (A=Y, Gd, and Nd) pyrochlores*, Phys. Rev. B **67**, 174406 (2003)

[43] G.Y. Guo, S. Murakami, T.-W. Chen, and N. Nagaosa, *Intrinsic Spin Hall Effect in Platinum: First-Principles Calculations*, Phys. Rev. Lett. **100**, 096401 (2008).

[44] G. Y. Guo, *Ab initio calculation of intrinsic spin Hall conductivity of Pd and Au*, J. Appl. Phys. **105**, 07C701 (2009).

[45] F. Freimuth, S. Blügel, and Y. Mokrousov, *Anisotropic Spin Hall Effect from First Principles*, Phys. Rev. Lett. **105**, 246602 (2010).